Mesoscale Dynamics

By Yuh-Lang Lin

[Lin, Y.-L., 2007: *Mesoscale Dynamics*. Cambridge University Press.]

3. Basic wave dynamics
Chapter 3 Basic wave dynamics

3.1 Introduction

When an air parcel is displaced from its initial position, a *restoring force* may cause it to return to its initial position. In doing so, inertia will cause the air parcel to overshoot and pass its initial equilibrium position moving in the opposite direction from that in which it is initially displaced, thereby creating an oscillation around the equilibrium position. Concurrently, a wave is produced that propagates from this source region to another part of the fluid system, which is the physical *medium of wave propagation*. A physical restoring force and a medium for propagation are the two fundamental elements of all wave motion in solids, liquids, and gases, including atmospheric waves, oceanic waves, sound (acoustic) waves, wind-induced waves, seismic waves, or even traffic density waves. The ultimate behavior of the wave is dictated by the individual properties of the restoring force responsible for wave generation and the medium through and by which the wave propagates energy and momentum.

From scaling arguments of the so-called primitive equations based on horizontal scales of fluid motion, some of the more important categories of waves observed in the atmosphere may be classified as follows (Table 3.1): (a) sound (acoustic) waves, (b) mesoscale waves, and (c) planetary (Rossby) waves. In this chapter, mesoscale waves are defined in a more general manner, referring to waves that exist and propagate in the atmosphere with a mesoscale wavelength.

Thus, mesoscale waves include pure gravity waves and inertia-gravity waves, instead of being limited to some long-lasting waves as are also defined in the literature. A more detailed classification of these waves and their probable restoring or wave generation forces are summarized in Table 3.1. Each group of waves exhibits multiple flow regimes. For example, pure gravity waves may be further categorized as either vertically propagating waves or evanescent waves, depending upon whether the wave energy is free to propagate vertically. The restoring forces for pure gravity waves and inertia oscillations are the buoyancy force ($-g\rho'/\bar{\rho}$ or $g\theta'/\bar{\theta}$) and Coriolis force, respectively. Sound waves derive their oscillations from longitudinal compression and expansion, while planetary waves derive their oscillations from the meridional variation of the Coriolis force or β effect. The compression force, buoyancy force, Coriolis force, and variation of Coriolis forces are often represented by c_s, N^2, f, and β in governing equations. The compression force, buoyancy force, Coriolis force, and variation of Coriolis force are normally represented by c_s, N^2, f, and β, respectively.

Restoring forces may also combine and work together to generate mixed waves, such as inertia-gravity waves, mixed acoustic-gravity waves, and mixed Rossby-gravity waves. Inertia-gravity waves are also known as Poincaré waves on the ocean surface and as boundary Kelvin waves along a rigid, lateral boundary such as a shoreline or coast. The oscillation period of the waves is determined by the strength of the restoring force and characteristics in the wave medium. The presence of mesoscale waves in the atmosphere and oceans can be inferred from (a) thermodynamic soundings, (b) microbarograph pressure traces, (c) visible and infrared satellite images, (d) radar echoes, and (e) vertical wind profilers. Data obtained from these sources and instruments may be used to help predict mesoscale wave

generation and propagation, as well as to help explain the development and subsequent evolution of a variety of mesoscale scale weather phenomena associated with the passage of these waves.

In previous studies of large-scale dynamics and numerical weather prediction (NWP), mesoscale and sound waves were often regarded as undesirable "noise", since they often appear as small perturbations or disturbances embedded in the large-scale flow, and their presence can even trigger numerical instabilities in an operational forecast model if the grid interval of the NWP model is not sufficiently small. Therefore, they are normally filtered out from the primitive equations. However, mesoscale waves do have major dynamical impacts on the atmosphere, such as:

(a) The spectral transfer of energy between large and small scale motions,

(b) The vertical and horizontal transport of energy and momentum from one region of the atmosphere to another,

(c) The generation of disturbances, such as mountain waves and clear-air turbulence (CAT), that can adversely affect airflow, weather, and aviation safety etc.,

(d) The triggering of hydrodynamic instabilities that lead to the generation of severe weather, and

(e) The generation of convective storms and the organization of individual convective cells or elements into larger-scale convective systems.

In order to understand the above mentioned atmospheric processes and better predict them, it is essential to understand the dynamics of mesoscale waves.

In this chapter, we will derive the governing equations and dispersion relationships for mesoscale waves, based on linearized equations derived from perturbation theory, and then discuss wave properties for different flow regimes. Since linear wave theory provides a powerful tool that helps to analyze and predict the variety of mesoscale waves observed in the atmosphere and those predicted by numerical models, we will restrict ourselves to this mathematical framework almost exclusively. In order to help readers understand basic wave properties, we will begin the discussion with shallow water waves and sound waves. In a structured atmosphere, mesoscale waves, just as synoptic or planetary-scale waves, may be reflected, transmitted, and even over-reflected from certain internal boundaries. These properties will be discussed in the later part of the chapter. Wave generation, propagation, and maintenance mechanisms will also be presented in Chapter 4.

3.2 Basic wave properties

With the Boussinesq approximation, the linearized perturbation equations, (2.2.14) – (2.2.18), can be combined into a single equation for the vertical velocity *w'*,

$$\begin{aligned}&\frac{D}{Dt}\left\{\frac{D^2}{Dt^2}\nabla^2 w' + f^2 w'_{zz} - \left(U_{zz}\frac{D}{Dt} + fV_{zz}\right)w'_x - \left(V_{zz}\frac{D}{Dt} - fU_{zz}\right)w'_y + N^2\nabla_H^2 w' + 2f\left(U_z w'_{yz} - V_z w'_{xz}\right)\right\}\\ &+2fU_zV_z\left(w'_{xx} - w'_{yy}\right) + 2f\left(V_z^2 - U_z^2\right)w'_{xy} - 2f^2\left(U_z w'_{xz} + V_z w'_{yz}\right) = \frac{g}{c_p T_o}\frac{D}{Dt}\nabla_H^2 q',\end{aligned} \tag{3.2.1}$$

Where $D/Dt = \partial/\partial t + U\partial/\partial x + V\partial/\partial y$. This equation governs the small-amplitude vertical velocity *w'* in a mesoscale system, which may contain the following mechanisms: (a) pure gravity and inertia-gravity wave generation, (b) static instability, (c) shear instability, (d) symmetric instability, and (e) baroclinic instability (Emanuel and Raymond, 1984). For different flow regimes, the Boussinesq form of (2.2.14) - (2.2.18) may reduce to different approximate equations, which will be further discussed in Sections 3.5 and 3.6.

Regardless of the restoring forces and propagation media, wave motions may be characterized by several fundamental properties, such as wave frequency, wave number, phase speed, group velocity, and dispersion relationship. Note that the dispersion relationship relates the wave frequency to the wave number. The period of oscillation (τ) of a wave determines the wave frequency ($\omega = 2\pi/\tau$), while the horizontal and vertical spatial scales (L_x, L_y, L_z) of a wave determine its horizontal and vertical wave numbers ($k = 2\pi/L_x;\ l = 2\pi/L_y;\ m = 2\pi/L_z$). A wave may be characterized by its amplitude and phase, φ = Re{A exp[$i(kx + ly + mz - \omega t - \alpha)$]}, where φ represents any of the dependent flow variables, *Re* means the real part, A the amplitude, $kx + ly + mz - \omega t - \alpha$ the phase, and α the phase angle. The phase angle is determined by the initial position of the wave. Lines of constant phase, such as wave crests, troughs, or any other particular part of the wave propagate through the fluid medium at a speed called the phase speed. Phase speeds in *x*, *y*, and *z* directions, are respectively given by

$$c_{px} = \omega/k; \quad c_{py} = \omega/l; \quad \text{and } c_{pz} = \omega/m. \tag{3.2.2}$$

If an observed or experimental set of data is available, the phase speed of a wave may be estimated by determining and tracing a constant phase of the wave.

In a geophysical fluid system such as the atmosphere, waves normally are very complicated in form, due to the superposition of wave components with different wavelengths and their nonlinear interactions, and cannot be represented by a simple, single sinusoidal wave. However, a small-amplitude wave with any shape can be approximately represented by a linear superposition of wave trains of different wave numbers, i.e. a Fourier series of sinusoidal components. For example, a wave in the *x* direction may be decomposed into sinusoidal components of the form,

$$\varphi(x) = \sum_{n=1}^{\infty} \left(A_n \sin k_n x + B_n \cos k_n x \right), \tag{3.2.3}$$

where the Fourier coefficients A_n and B_n are determined by

$$A_n = \frac{2}{L} \int_0^L \varphi(x) \sin \frac{2\pi n x}{L} dx \,, \tag{3.2.4}$$

$$B_n = \frac{2}{L} \int_0^L \varphi(x) \cos \frac{2\pi n x}{L} dx \,. \tag{3.2.5}$$

The *n*th Fourier component or nth harmonic of the wave function φ_n is defined as $A_n \sin k_n x + B_n \cos k_n x$. In deriving (3.2.4) and (3.2.5), we have used the orthogonality relationships,

$$\int_0^L \sin \frac{2\pi n x}{L} \cos \frac{2\pi m x}{L} dx = 0, \qquad \text{for all } n, m > 0 \,,$$

$$\int_0^L \sin \frac{2\pi\, n x}{L} \sin \frac{2\pi\, m x}{L} dx = \begin{Bmatrix} 0, & n \neq m \\ L/2, & n = m \end{Bmatrix}, \text{ and}$$

$$\int_0^L \cos\frac{2\pi\, nx}{L}\cos\frac{2\pi\, mx}{L}dx = \begin{Bmatrix} 0, & n \neq m \\ L/2, & n = m \end{Bmatrix}. \qquad (3.2.6)$$

If a wave is composed of a series of Fourier components of different wavelengths, then the phase speed for each individual component may also be different, according to (3.2.2). If the phase speed is independent of wave number or wavelength, then the wave will retain its initial shape and remain coherent as it propagates throughout the fluid medium. This type of wave is *nondispersive*. On the other hand, if the phase speed is a function of wave number or wavelength, then the wave will not be able to retain its initial shape and remain coherent as it propagates in the medium since each Fourier component is propagating at a different phase speed. In other words, the wave is *dispersive*. Thus, it becomes clear that the relationship between wave frequency and wave number determines whether or not the wave is dispersive.

Although visually, a dispersive wave may look like it is dissipative, dispersion and dissipation are completely different physical processes. In a dissipative, but nondispersive wave, every Fourier component of the wave propagates at the same speed, while the wave amplitude decreases. Thus, individual wave groups preserve their phase (shape) during propagation. If the wave is nondispersive, then the wave pattern moves throughout the medium without any change in shape of the initial waveform. This means that the *phase velocity* of the individual wave crests (c_p) is equal to the *group velocity* of the slow-varying modulations or the envelope of Fourier wave components (c_g). The concept of group velocity is illustrated in Fig. 3.1, in which the simple group of two superimposed sinusoidal waves, represented by the wave function φ = Re{A exp[i((k+Δk)x–(ω+$\Delta\omega$)t)]+exp[i((k–Δk)x–(ω–$\Delta\omega$)t)]}, propagates at the

speed $\Delta\omega/\Delta k$. This velocity approaches $\partial\omega/\partial k$, which is defined as the group velocity in the *x* direction, as Δk approaches 0. Thus, the group velocity represents the velocity the slow-varying modulation of a wave propagates, which is given by the relation

$$\boldsymbol{c_g} = c_{gx}\boldsymbol{i} + c_{gy}\boldsymbol{j} + c_{gz}\boldsymbol{k} = \frac{\partial\omega}{\partial k}\boldsymbol{i} + \frac{\partial\omega}{\partial l}\boldsymbol{j} + \frac{\partial\omega}{\partial m}\boldsymbol{k}. \qquad (3.2.7)$$

From the incompressible continuity equation, one can show that

$$\boldsymbol{k}\cdot\boldsymbol{V}' = 0, \qquad (3.2.8)$$

where $\boldsymbol{k}$ = (*k, l, m*) is the *wave number vector*. For two-dimensional plane waves (e.g., *l* = 0), the above equation indicates that the wave motion or oscillation of fluid parcels is perpendicular to the wave number vector. At any instant t_o, a *wave front* is defined by setting the phase ($\boldsymbol{k}\cdot\boldsymbol{x} - \omega t - \alpha$) to be constant, which indicates that a family of parallel planes is normal to the wave number vector $\boldsymbol{k}$. As time proceeds, these planes move with the phase speed in the direction $\boldsymbol{k}$. Notice that the phase velocity can be derived as

$$\boldsymbol{c} = \omega\boldsymbol{k}/k^2. \qquad (3.2.9)$$

That is, the phase velocity $\boldsymbol{c}$ is parallel to $\boldsymbol{k}$. As will be discussed in Section 3.6, inertia-gravity waves are an example of *transverse waves* because the fluid particle motion, $\boldsymbol{V}'$, is perpendicular to the phase velocity (Fig. 3.9 or Fig. 3.10a), as indicated by (3.2.8). Note that the phase speeds in the *x* and *z* directions do not comprise the phase velocity. That is,

$$\boldsymbol{c} \neq (\omega/k, \omega/l, \omega/m). \qquad (3.2.10)$$

For sound waves (Section 3.3), it can be shown that

$$\boldsymbol{k} \cdot \boldsymbol{V}' \neq 0. \qquad (3.2.11)$$

Thus, sound waves are an example of *longitudinal waves*.

3.3 Sound waves

Sound (acoustic) waves derive their oscillations from the compression and expansion of the medium due to the compression force. Consider one-dimensional ($\partial/\partial y = \partial/\partial z = 0$), small-amplitude, adiabatic perturbations in a non-rotating, inviscid, uniform (no basic wind shear) flow governed by (2.2.14) – (2.2.18),

$$\frac{\partial u'}{\partial t} + U\frac{\partial u'}{\partial x} + \frac{1}{\bar{\rho}}\frac{\partial p'}{\partial x} = 0, \qquad (3.3.1)$$

$$\frac{\partial p'}{\partial t} + U\frac{\partial p'}{\partial x} + \gamma \bar{p}\frac{\partial u'}{\partial x} = 0. \qquad (3.3.2)$$

The above two equations may be combined into a single equation for *p'*,

$$\left(\frac{\partial}{\partial t} + U\frac{\partial}{\partial x}\right)^2 p' - c_s^2 \frac{\partial^2 p'}{\partial x^2} = 0, \qquad (3.3.3)$$

where $c_s^2 = \gamma R\bar{T}$. Assuming a wave-like solution,

$$p(x,t) = p_o e^{i(kx-\omega t)} = p_o[\cos(kx-\omega t) + i\sin(kx-\omega t)],$$

and substituting it into (3.3.3) leads to

$$\omega = (U \pm c_s)k. \qquad (3.3.4)$$

For brevity, we omit the Re{ } notation in the wave-like solution, but it is to be understood that only the real part of the above solution has physical significance. The above method of the assumption of wave-like solutions for the small-amplitude perturbations is also referred to as the *method of normal modes*. The above equation is the dispersion relation for sound waves, which relates the wave frequency ω to the horizontal wave number *k*. From (3.3.4), we may obtain the horizontal phase speeds, which are given by

$$c_p = \frac{\omega}{k} = U \pm c_s . \qquad (3.3.5)$$

The above equation represents phase speeds of the downstream ($U + c_s$) and upstream ($U - c_s$) propagating sound waves, which are simultaneously being advected by the basic wind *U*. Sound waves are nondispersive since their phase speeds are independent of wave number. This nondispersive property of sound waves may also be verified by showing that the group velocities for these waves c_g are identical to their phase speeds c_p.

Consider a semi-infinite tube filled with gas whose right-hand side extends to infinity and whose left-hand side is confined by a piston. When the gas is alternatively compressed and expanded by oscillating the piston in and out of the left hand side of the semi-infinite tube, an air parcel located adjacent to the piston will be forced to oscillate back and forth about its equilibrium position due to the oscillating horizontal pressure gradient and, concurrently, a sound wave will be excited that propagates toward the right at the speed $c_s = \sqrt{\gamma R \overline{T}}$. In a dry, isothermal atmosphere with a constant temperature of 300 K, a one-dimensional acoustic wave has a phase speed and group velocity of approximately 347 ms^{-1} (~ 776 mph).

In fact, the general solution of (3.3.3) may be written as,

$$p' = F[x + (U + c_s)t] + F[x + (U - c_s)t], \tag{3.3.6}$$

where F is any arbitrary function whose amplitude is one-half that of the initial disturbance, and whose shape is identical to that of the initial disturbance. In a quiescent fluid, the first and second terms on the right hand side of (3.3.6) represent the leftward and rightward propagating sound waves, respectively. Since sound waves do not play significant dynamic roles in affecting most atmospheric motions, they are often eliminated from the primitive equations - in particular those that are commonly employed in most current operational NWP models. Although sound waves may have no particular relevance to atmospheric motions in the troposphere that are responsible for "weather", a special class of waves called *Lamb waves* has been observed. These waves can propagate horizontally in an isothermal atmosphere in the absence of vertical motion. Lamb waves, as well as sound waves and gravity waves, can be generated by latent heat release in a convective storm (e.g., Nicholls and Pielke 2000). In a two-dimensional ($\partial / \partial y = 0$), adiabatic, hydrostatic, non-rotating, inviscid, isothermal atmosphere with no vertical motion and basic wind shear, small-amplitude motions are governed by (2.2.14) – (2.2.18) reduced to (3.3.1), (3.3.2), and

$$\frac{1}{\bar{\rho}}\left(\frac{\partial p'}{\partial z} + \frac{p'}{H}\right) = g\frac{\theta'}{\bar{\theta}}, \tag{3.3.7}$$

$$\frac{\partial \theta'}{\partial t} + U\frac{\partial \theta'}{\partial x} = 0. \tag{3.3.8}$$

Note that in an isothermal atmosphere, the scale height, $H = c_s^2 / g$, is a constant. Equations (3.3.7) and (3.3.8) may be combined to yield an equation that, when coupled with (3.3.3), forms the set of equations governing the evolution of Lamb waves.

3.4 Shallow water waves

Shallow water waves propagate horizontally along a water or ocean surface or along an interfacial boundary between two layers of fluid with distinctly different densities. Although this type of wave is observed more often in the oceans and lakes, they are also occasionally observed in the atmosphere. For example, the mesoscale waves generated below a thunderstorm that subsequently propagate along a temperature inversion capping a layer of very dense cold air produced by evaporative cooling produced by the storm, may be characterized and treated mathematically as shallow water waves. Another example is the internal hydraulic jump occurring over the lee slope of a mountain, as that shown in Fig. 3.5. Shallow water wave theory has also been applied to understand other weather systems, such as the propagation of tropical cyclones and tropical waves.

Consider a non-rotating, hydrostatic, two-layer fluid system with constant densities ρ_1 and ρ_o in the upper and lower layers, respectively, and assume that $\rho_1 < \rho_o$ (stably stratified) and that there exist no horizontal pressure gradients in the upper layer (Fig. 3.2). This two-layer shallow water system is governed by the following reduced forms of the horizontal momentum equations and the vertically integrated continuity equation,

$$\frac{\partial u}{\partial t} + u\frac{\partial u}{\partial x} + v\frac{\partial u}{\partial y} = -g'\frac{\partial (h + h_s)}{\partial x}, \tag{3.4.1}$$

$$\frac{\partial v}{\partial t} + u\frac{\partial v}{\partial x} + v\frac{\partial v}{\partial y} = -g'\frac{\partial (h + h_s)}{\partial y}, \tag{3.4.2}$$

$$\frac{\partial h}{\partial t} + u\frac{\partial h}{\partial x} + v\frac{\partial h}{\partial y} + h\left(\frac{\partial u}{\partial x} + \frac{\partial v}{\partial y}\right) = 0, \tag{3.4.3}$$

where h is the instantaneous depth of the fluid. The above three equations, corresponding to (A3.1.9), (A3.1.10), and (A3.1.14), respectively, are derived in Appendix 3.1. Decomposing u, v, and h into basic state and perturbation, $u = U + u'$, $v = V + v'$, and $h = H + h' - h_s$, and substituting them into (3.4.1) – (3.4.3) leads to the following perturbation equations:

$$\frac{\partial u'}{\partial t} + (U + u')\frac{\partial u'}{\partial x} + (V + v')\frac{\partial u'}{\partial y} + g'\frac{\partial h'}{\partial x} = 0, \tag{3.4.4}$$

$$\frac{\partial v'}{\partial t} + (U + u')\frac{\partial v'}{\partial x} + (V + v')\frac{\partial v'}{\partial y} + g'\frac{\partial h'}{\partial y} = 0, \tag{3.4.5}$$

$$\begin{aligned}\frac{\partial h'}{\partial t} + (U + u')\frac{\partial h'}{\partial x} + (V + v')\frac{\partial h'}{\partial y} + (H + h' - h_s)\left(\frac{\partial u'}{\partial x} + \frac{\partial v'}{\partial y}\right) = \\ (U + u')\frac{\partial h_s}{\partial x} + (V + v')\frac{\partial h_s}{\partial y}.\end{aligned} \tag{3.4.6}$$

Note that H is the undisturbed upstream layer depth, h_s is the height of the bottom topography, h' is the vertical displacement from H. Thus, h_s is no longer included in the horizontal pressure gradient forces in the momentum equations (3.4.4) and (3.4.5). However, in the system of perturbation equations, (3.4.4) – (3.4.6), h_s serves as a forcing term for the vertical velocity $w' = Dh'/Dt$ in the vertically integrated mass continuity equation, (3.4.6).

For simplicity, consider the special case of small-amplitude (linear) perturbations in a one-layer fluid with a flat bottom and with $V = 0$. This system may be used as a first approximation of the air-water system since $\rho_{air} << \rho_{water}$. These assumptions yield $\Delta\rho = \rho_o - \rho_1 \approx \rho_o$, where $\rho_o = \rho_{water}$, $\rho_1 = \rho_{air}$, and $g' = g$. Under these assumptions, (3.4.4) – (3.4.6) become

$$\frac{\partial u'}{\partial t} + U\frac{\partial u'}{\partial x} + g\frac{\partial h'}{\partial x} = 0, \tag{3.4.7}$$

$$\frac{\partial v'}{\partial t} + U\frac{\partial v'}{\partial x} + g\frac{\partial h'}{\partial y} = 0, \tag{3.4.8}$$

$$\frac{\partial h'}{\partial t} + U\frac{\partial h'}{\partial x} + H\left(\frac{\partial u'}{\partial x} + \frac{\partial v'}{\partial y}\right) = 0. \tag{3.4.9}$$

The above set of equations can be combined into a wave equation governing the free surface displacement perturbation h'

$$\left(\frac{\partial}{\partial t} + U\frac{\partial}{\partial x}\right)^2 h' - (gH)\left(\frac{\partial^2 h'}{\partial x^2} + \frac{\partial^2 h'}{\partial y^2}\right) = 0\,. \tag{3.4.10}$$

Applying the method of normal modes with $h' = A\exp[i(kx - \omega t)]$ and substituting it into the two-dimensional form of (3.4.10) (i.e., with $\partial / \partial y = 0$), we obtain the dispersion relationship for two-dimensional shallow water waves,

$$c = U \pm \sqrt{gH} \,. \qquad (3.4.11)$$

With no basic flow, the above equation indicates that the solution to (3.4.10) consists of a leftward and a rightward propagating shallow-water wave along the free surface of the fluid with the shallow-water wave (phase) speeds of $-\sqrt{gH}$ and $\sqrt{gH}$, respectively. With a basic flow, these two waves are advected by the basic flow speed (*U*). Since the phase speeds are independent of wave number, these two-dimensional shallow-water waves are nondispersive. It is straightforward to show that the group velocity is identical to the phase velocity in this system. In fact, we may obtain this conclusion directly from the general solution to the wave equation, namely,

$$h'(t,x) = \frac{1}{2} f[x + (U + \sqrt{gH})t] + \frac{1}{2} f[x + (U - \sqrt{gH})t], \qquad (3.4.12)$$

where $f(x)$ is the initial disturbance and f is any arbitrary function. The function represented by $(1/2)f$ will preserve the shape of the initial disturbance, but its amplitude will only be half that of the initial disturbance. An example for this is the shallow-water waves excited by the horizontal pressure gradient force along the free surface associated with the initial disturbance, which physically represents a localized, mesoscale high pressure system,

$$h'(x) = \frac{h_o b^2}{x^2 + b^2}, \qquad (3.4.13)$$

are represented mathematically as,

$$h'(x,t)=\frac{(h_o/2)\,b^2}{[x+(U+\sqrt{gH})t]^2+b^2}+\frac{(h_o/2)\,b^2}{[x+(U-\sqrt{gH})t]^2+b^2}\,. \qquad (3.4.14)$$

Equation (3.4.13) is called a *bell-shaped function* or the *Witch of Agnesi*, in which h_o and b are the maximum amplitude and half-width of the initial disturbance, respectively. Note that the waves generated have the same bell-shaped form but with their amplitude reduced to half that of the initial disturbance.

The equation for the total perturbation energy for a three-dimensional shallow water system can be derived,

$$\left(\frac{\partial}{\partial t}+U\frac{\partial}{\partial x}\right)\left[\frac{1}{2}\rho H(u'^2+v'^2)+\frac{1}{2}\rho g h'^2\right]+\rho g H\left[\frac{\partial}{\partial x}(u'h')+\frac{\partial}{\partial y}(v'h')\right]=0\,. \qquad (3.4.15)$$

The first term inside the first square bracket is the perturbation kinetic energy, and the second term is the perturbation potential energy. The above equation indicates that the change in total perturbation energy per unit area is simply caused by the convergence or divergence of the mass flux.

Different flow regimes may result from different upstream flow conditions. For a two-dimensional, non-rotating, small-amplitude shallow water flow over an obstacle, the wave equation governing the evolution in vertical displacement can be derived

$$\left(\frac{\partial}{\partial t}+U\frac{\partial}{\partial x}\right)^2 h'-(gH)\frac{\partial^2 h'}{\partial x^2}=U\left(\frac{\partial}{\partial t}+U\frac{\partial}{\partial x}\right)\frac{\partial h_s}{\partial x}\,. \qquad (3.4.16)$$

A steady state solution for (3.4.16) can be found

$$h'(x)=\left(\frac{F^2}{F^2-1}\right)h_s(x)\,;\quad F\equiv\frac{U}{\sqrt{gH}}\,, \qquad (3.4.17)$$

where F is the *shallow-water Froude number* that represents the ratio of the advection flow speed to the *shallow water wave phase speed*. The Froude number also represents the ratio between the square-root of the kinetic and potential energies of the undisturbed, upstream basic flow. Equation (3.4.17) implies that

$$h' \propto \begin{cases} h_s & \text{for } F > 1 \\ -h_s, & \text{for } F < 1 \end{cases} . \qquad (3.4.18)$$

The above equation indicates that if $F > 1$ far upstream, $h'(x)$ follows the shape of $h_s(x)$. The interface or free surface will bow upwards over the obstacle as shown in Fig. 3.3a. That is, physically, the upstream flow has enough kinetic energy to overcome the potential energy barrier associated with the obstacle. This flow regime is called *supercritical flow*. On the other hand, when $F < 1$, $h'(x)$ decreases as $h_s(x)$ increases, as the perturbation flow converts its potential energy into enough kinetic energy to surmount the obstacle (Fig. 3.3e). Over the peak of the obstacle, the fluid reaches its maximum speed, as implied from (3.4.17). This flow regime is called *subcritical flow*. When the flow is supercritical $(F > 1)$, small-amplitude disturbances cannot propagate upstream against the basic flow, and any obstacle along the bottom will tend to produce a purely local disturbance. When the flow is subcritical $(F < 1)$, shallow water waves are able to propagate upstream since the shallow water wave speed is larger than the basic wind speed. The steady state effect of this response is to effectively increase the layer depth upstream, which increases the potential energy of the incoming flow. The potential energy is then converted into kinetic energy as the fluid surmounts the obstacle. Thus, the fluid reaches its maximum speed, and the water surface dips down over the peak of the obstacle creating a *Bernoulli* or *venturi* effect. The relationship between u' and h' can be derived,

$$\frac{u'}{U} = -\left(\frac{1}{F^2}\right)\frac{h'}{H}, \qquad (3.4.19)$$

which indicates that the flow decelerates (accelerates) over a hump for a supercritical (subcritical) flow. In addition to F, (3.4.17) indicates that the nondimensional mountain height M ($\equiv h/H$, where h is the mountain height) also serves as a control parameter of the shallow-water flow over a bottom topography. In other words, the flow behavior of the shallow-water system is controlled by F and M.

The above discussion on wave characteristics is based on the steady-state solution (3.4.17). In transient flow, additional flow regimes may occur. Based on the nondimensional control parameters F and M, five different flow regimes can be identified in transient, single-layer shallow water flow over an isolated obstacle (Fig. 3.3; Houghton and Kasahara 1968; Long 1970): (a) supercritical flow, (b) flow with both upstream and downstream propagating hydraulic jumps, (c) flow with an upstream propagating hydraulic jump and a downstream stationary hydraulic jump, (d) completely blocked flow, and (e) subcritical flow. As discussed above, in a supercritical flow with $F > 1$ everywhere, a fluid parcel has enough kinetic energy to ascend the obstacle, converting kinetic energy into potential energy. Consequently, the free surface rises symmetrically over the symmetric obstacle (Regime A, Fig. 3.3a). The fluid reaches its minimum speed over the top of the obstacle. As either F decreases or M increases, the upstream flow is partially blocked, and the flow response shifts to the regime in which both an upstream *hydraulic jump* (*bore*) and a downstream hydraulic jump form and propagate away from the obstacle as time proceeds (Regime B, Fig. 3.3b). In this case, the upstream flow is partially blocked and a transition from subcritical to supercritical flow regimes occurs over the peak of the obstacle. Very high velocities are produced along the lee slope of the obstacle, which may help

explain the occurrence of severe downslope winds for atmospheric flow over a mountain (Sec. 5.3), because the potential energy associated with the upstream flow is accumulated and converted into kinetic energy when the fluid passes over and descends the lee slope. Eventually, a steady state is established in the vicinity of the obstacle, and the shape of the free surface acquires a waterfall-like profile.

As F decreases further, the flow shifts to the regime in which an upstream hydraulic jump forms and propagates upstream, while the downstream hydraulic jump becomes stationary over the lee slope of the obstacle due to weaker advection associated with the incipient basic state flow (Regime C, Fig. 3.3c). Similar to Regime B, the upstream flow is also partially blocked. Both flow regimes B and C are characterized by high surface drag across the obstacle, as well as large flow velocities along the lee slope, and are referred to as the *transitional flow*. The *surface drag* is the pressure difference exerted by the shallow-water wave on the surface of the obstacle and is also called *mountain drag* or *form drag*.

For stationary mountain waves to exist in the atmosphere, the mountain must in some way be exerting a force against the flow so that the waves remain stationary. This force is called *mountain wave drag*, or *gravity wave drag*. Similar to Regime B, this transitional flow regime has also been used to help explain the formation of severe downslope windstorms. Figure 3.4a shows the severe downslope windstorm that occurred near Boulder, Colorado, on 11 January 1972 and a sketch (Fig. 3.4b) of shallow-water flow regime C that may represent the situation accompanying the 1972 Boulder windstorm. The severe downslope wind over the Front Range of the Rockies to the east of the Continental Divide reached a speed of over 60 ms^{-1}. The mechanisms thought responsible for producing

severe downslope winds will be discussed in Chapter 5. Figure 3.5 shows a photograph of an internal hydraulic jump occurring in the atmosphere along the eastern Sierra Nevada and Owens Valley, California. This type of flow ($F < 1$) is categorized as subcritical flow (Regime E, Fig. 3.3e), as discussed earlier. With a very small F and $M > 1$, the flow response falls into the regime of completely blocked flow (Regime D, Fig. 3.3d). In addition, there exists a region located to the upper left corner of flow Regime B in Fig. 3.3b, in which the flow may be either supercritical or partially blocked (i.e. with hydraulic jumps present), depending upon the initial conditions (Long 1970).

If the nonlinear terms in the governing equations are included, then *wave steepening* may occur. The nonlinear effects on wave steepening may be illustrated by imagining an elevated wave that is composed of several rectangular blocks with shorter blocks of fluid on top of longer blocks (Fig. 3.6a). Since the shallow water wave speed is proportional to the mean layer depth H, the speed of fluid particles in the upper layer will be greater than that in the lower layer. Thus, the wave front will have a tendency to steepen (Fig. 3.6b) and possibly overturn (Fig. 3.6c). Once overturning occurs, the fluid becomes statically unstable and turbulence will be induced.

In a rotating shallow water system, the Coriolis force becomes more and more important when the Rossby number decreases. In this situation, the fluid may undergo geostrophic adjustment to an initial disturbance, as briefly discussed in Chapter 1, to a scale determined by the Rossby radius of deformation, $\lambda_R = c / f = \sqrt{gH} / f$.

3.5 Pure gravity waves

Consider small-amplitude (linear) perturbations in a two-dimensional ($\partial/\partial y = 0$), inviscid, nonrotating, adiabatic, Boussinesq, uniform basic state flow with uniform stratification, (2.2.14) – (2.2.18) reduce to

$$\frac{\partial u'}{\partial t} + U\frac{\partial u'}{\partial x} + \frac{1}{\rho_o}\frac{\partial p'}{\partial x} = 0, \tag{3.5.1}$$

$$\frac{\partial w'}{\partial t} + U\frac{\partial w'}{\partial x} - g\frac{\theta'}{\theta_o} + \frac{1}{\rho_o}\frac{\partial p'}{\partial z} = 0, \tag{3.5.2}$$

$$\frac{\partial u'}{\partial x} + \frac{\partial w'}{\partial z} = 0, \tag{3.5.3}$$

$$\frac{\partial \theta'}{\partial t} + U\frac{\partial \theta'}{\partial x} + \frac{N^2\theta_o}{g}w' = 0, \tag{3.5.4}$$

where θ_o is a constant reference potential temperature, and $N^2 [\equiv (g/\theta_o)\partial\bar{\theta}/\partial z]$ is the square of the Boussinesq Brunt-Vaisala (buoyancy) frequency. Figure 3.7 illustrates the vertical oscillation of an air parcel in a stratified atmosphere with a Brunt-Vaisala frequency *N*. The total oscillation period is $2\pi/N$ (τ_b in the figure). The air parcel expands and cools while it ascends, and reaches its maximum expansion and coolest state at $t = \tau_b/4$. At this level, the air parcel density perturbation is the largest. It then descends due to negative buoyancy and overshoots passing its original level at $t = \tau_b/2$. The air parcel compresses and warms adiabatically while it descends, and reaches its maximum compression and warmest state at $t = 3\tau_b/4$. At this level, the air parcel density perturbation is the lowest. It then ascends due to positive buoyancy, and returns to its original level at $t = \tau_b$. For a two-dimensional, nonrotating fluid flow, there is no need to retain the meridional (*y*-) momentum equation in our system of equations, because *v*' will

keep its initial value for all time, as required by the reduced form of the y-momentum equation, namely, $\partial v'/\partial t + U\partial v'/\partial x = 0$. Note that the y-momentum equation needs to be kept if the fluid is two-dimensional and rotating since the initial v' will vary with time, although independent of y, due to the presence of the Coriolis force.

Equations (3.5.1) – (3.5.4) may be combined into a single equation for the vertical velocity w', which is a simplified form of the *Taylor-Goldstein equation* [(3.7.19)] in the absence of vertical wind shear,

$$\left(\frac{\partial}{\partial t} + U\frac{\partial}{\partial x}\right)^2\left(\frac{\partial^2 w'}{\partial x^2} + \frac{\partial^2 w'}{\partial z^2}\right) + N^2\frac{\partial^2 w'}{\partial x^2} = 0. \qquad (3.5.5)$$

Assuming a traveling sinusoidal plane wave solution of the form,

$$w' = \hat{w}(z)\ e^{i(kx-\omega t)}, \qquad (3.5.6)$$

and substituting it into (3.5.5) yields the following linear partial differential equation with constant coefficients, which governs the vertical structure of w',

$$\frac{\partial^2 \hat{w}}{\partial z^2} + \left(\frac{N^2}{\Omega^2} - 1\right)k^2\hat{w} = 0. \qquad (3.5.7)$$

In the above equation, $\Omega \equiv \omega - kU$ is the *intrinsic* (*Doppler-shifted*) *frequency* of the wave relative to the uniform basic state flow. Equation (3.5.7) has the following two solutions:

$$\hat{w} = A\,e^{ik\sqrt{N^2/\Omega^2 - 1}\,z} + B\,e^{-ik\sqrt{N^2/\Omega^2 - 1}\,z}, \quad \text{for } N^2/\Omega^2 > 1, \qquad (3.5.8)$$

and

$$\hat{w} = C\,e^{k\sqrt{1-N^2/\Omega^2}\,z} + D\,e^{-k\sqrt{1-N^2/\Omega^2}\,z}, \quad \text{for } N^2/\Omega^2 < 1. \qquad (3.5.9)$$

Equation (3.5.8) represents a vertically propagating wave because it is sinusoidal with height. As will be discussed in Section 4.4, term *A* represents a wave with upward energy propagation, while term *B* represents a wave with downward energy propagation. Thus, for waves generated by orography, term *B* is unphysical and has to be removed because the wave energy source is located at the surface, as required by the *radiation boundary condition*. On the other hand, term *C* of (3.5.9) represents wave amplitude increasing exponentially with height, while term *D* represents a wave whose amplitude decreases exponentially from the level of wave generation. Thus, for waves or disturbances generated by orography, term *C* is unphysical. This is also called the *boundedness condition*. Under this situation, term *D* represents an evanescent wave or disturbance, whose wave amplitude decreases exponentially with height. In other words, there exist two distinct flow regimes for pure gravity waves (i.e. v*ertically propagating waves* and *evanescent waves*) in the atmosphere, which are determined respectively by the following criteria:

$$N^2/\Omega^2 > 1 \quad \text{and} \quad N^2/\Omega^2 < 1. \tag{3.5.10}$$

The above two pure gravity wave flow regimes can be understood by considering steady state responses of stably stratified airflow over a sinusoidal topography. In this particular case, $\Omega^2 = k^2U^2$. When $N^2/\Omega^2 > 1$, we have $2\pi/N < L/U$, where $L = 2\pi/k$ is the dominant horizontal wavelength of the sinusoidal topography. Note that $2\pi/N$ is the buoyancy oscillation period and that L/U is the advection time an air parcel takes to cross over the mountain. Thus, fluid particles take less time to oscillate in the vertical, compared to the horizontal advection time required to pass over the mountain. This allows the wave energy to propagate vertically (Fig. 3.8a). On the other hand, when $N^2/\Omega^2 < 1$ or $2\pi/N > L/U$, fluid particles do not have enough time to oscillate vertically because the time required

for the particles to be advected over the mountain is shorter. Therefore, the wave energy cannot freely propagate vertically, and it is preferentially advected downstream, remaining near the Earth's surface (Fig. 3.8b). This type of wave or disturbance is also referred to as an evanescent wave or a *surface trapped wave*.

If the stratification of the fluid is uniform and the disturbance is sinusoidal in the vertical, then $\hat{w}$ may be written as $\hat{w} = w_o e^{imz}$, where w_o and m are the wave amplitude and vertical wave number, respectively. Substituting $\hat{w}$ into (3.5.7) yields the dispersion relationship for pure gravity waves,

$$\Omega = \frac{\pm Nk}{\sqrt{k^2 + m^2}}. \qquad (3.5.11)$$

For a quiescent fluid ($U = 0$), the above equation reduces to

$$\omega = \frac{\pm Nk}{\sqrt{k^2 + m^2}}, \qquad (3.5.12)$$

or

$$\frac{\omega}{N} = \frac{\pm k}{\sqrt{k^2 + m^2}} = \pm \cos\alpha, \qquad (3.5.13)$$

where α is the angle ($|\alpha| \le \pi/2$) between the wave number vector $\boldsymbol{k} = (k, m)$ and the x-axis. While the wave number vector is oriented in the same direction as the phase speed vector ($\boldsymbol{c}_p$ in Fig. 3.9), the wave front is oriented perpendicular. Fluid parcels oscillate in a direction perpendicular to the total wave number vector, as indicated by the incompressible continuity equation, $\boldsymbol{k} \cdot \boldsymbol{V}' = 0$. Therefore, the wave fronts or rays associated with particle oscillations tilt at an angle α with respect to the vertical. This characteristic behavior of nonrotating internal gravity waves has

been verified in water tank experiments (Mowbray and Rarity 1967). For a given stratification, waves with constant $\omega < N$ propagate at a fixed angle to the horizontal axis, which is independent of the wavelength.

From (3.5.12), we may obtain the horizontal and vertical phase velocities,

$$c_{px} = \frac{\omega}{k} = \frac{\pm N}{\sqrt{k^2 + m^2}}; \quad c_{pz} = \frac{\omega}{m} = \frac{\pm kN}{m\sqrt{k^2 + m^2}} \tag{3.5.14}$$

These expressions indicate that pure gravity waves are dispersive in both the *x* and *z* directions because both c_{px} and c_{pz} depend on wave number. The group velocities can be derived from (3.5.12),

$$c_{gx} = \frac{\partial \omega}{\partial k} = \frac{\pm m^2 N}{\left(k^2 + m^2\right)^{3/2}}; \quad c_{gz} = \frac{\partial \omega}{\partial m} = \frac{\mp kmN}{\left(k^2 + m^2\right)^{3/2}}. \tag{3.5.15}$$

Note that c_{px} and c_{gx} are directed in the same direction, while c_{pz} and c_{gz} are directed in opposite directions. This is also shown in Fig. 3.9. Due to these peculiar properties of internal gravity waves, the implementations for lateral and upper boundary conditions associated with mesoscale numerical models that resolve these waves must be carefully configured. Briefly speaking, a horizontal advection equation, $\partial\varphi/\partial t + c_{px}\partial\varphi/\partial x = 0$, where φ represents any prognostic dependent variable, can be applied at the lateral boundaries and can be implemented to help advect the wave energy out of the lateral boundary of the computational domain. On the other hand, a vertical advection equation, $\partial\varphi/\partial t + c_{pz}\partial\varphi/\partial z = 0$ (with $c_{pz} > 0$), cannot advect the wave energy out of the upper boundary since the wave energy will propagate downward back into the computational domain as c_{gz} is negative. The numerical radiation boundary

conditions will be discussed in more detail in Section 13.2, while the details of the Sommerfeld (1949) radiation boundary condition will be discussed in Section 4.4.

Due to the fact that only the real part of the solution is physical, (3.5.6) and $\hat{w}(z) = w_o \exp(imz)$ can be combined in the form,

$$w' = \mathrm{Re}\left(w_o e^{i(kx+mz-\omega t)} \right) = w_r \cos(kx+mz-\omega t) - w_i \sin(kx+mz-\omega t), \qquad (3.5.16)$$

where w_r and w_i are the real and imaginary parts of w_o, respectively. Substituting w' into (3.5.1) – (3.5.4) with $U = 0$ leads to the *polarization relations*

$$u' = -(m/k)\left[w_r \cos(kx+mz-\omega t) - w_i \sin(kx+mz-\omega t) \right], \qquad (3.5.17a)$$

$$p' = -\left(\rho_o \omega m / k^2 \right)\left[w_r \cos(kx+mz-\omega t) - w_i \sin(kx+mz-\omega t) \right], \qquad (3.5.17b)$$

$$\theta' = \left(\theta_o N^2 / g\omega \right)\left[w_r \sin(kx+mz-\omega t) + w_i \cos(kx+mz-\omega t) \right]. \qquad (3.5.17c)$$

The above relationships are also shown in Fig. 3.9 for the case where $k > 0$, $m < 0$, and $\omega > 0$. The wave frequency is assumed to be positive, in order to avoid redundant solutions. For $k > 0$, $m < 0$, and $\omega > 0$, (3.5.17a) indicates that u' is in phase with w', which is shown in Fig. 3.9 by fluid oscillating toward the right in regions of upward motion. Equation (3.5.17b) indicates that p' is also in phase with w'. Thus, high (low) pressure is produced in regions of upward (downward) motion. Equation (3.5.17c) indicates that θ' is out of phase with w' by $\pi/2$ (90^o). Fluid particles lose (gain) buoyancy in regions of upward (downward) motion, according to (3.5.4) with $U = 0$. Therefore, the least buoyant (coldest) fluid parcels (denoted by C in t_1 of Fig. 3.9) will move toward regions of maximum upward

motion. That is, internal gravity waves will move in the direction of phase propagation (toward the lower right corner of the figure), as denoted by $\boldsymbol{c}_p$ in the figure.

Returning to the vertical structure solutions, (3.5.8) and (3.5.9), there are two extreme cases that merit further discussion. When $N^2 >> \Omega^2$, the buoyancy oscillation period ($2\pi / N$) is much shorter than the oscillation period of the disturbance ($2\pi / \omega$) or the advection time (L/U). Therefore, the wave energy will propagate purely in the vertical direction. In this situation, constant phase lines and group velocities are oriented vertically, while the total wave number vector is oriented horizontally. In this special flow regime, often referred to as the *hydrostatic gravity wave regime*, the vertical momentum equation (3.5.2) reduces to its hydrostatic form,

$$\frac{1}{\rho_o}\frac{\partial p'}{\partial z} = g\frac{\theta'}{\theta_o}. \qquad (3.5.18)$$

This implies that the vertical pressure gradient force is in balance with the buoyancy force in the *z* direction. In other words, vertical acceleration Dw'/Dt plays an insignificant role in wave propagation. It can be shown from (3.5.8) that the waves repeat themselves in the vertical direction without losing their amplitude and have a wavelength of $2\pi\Omega/kN$ for a steady state flow. For hydrostatic gravity waves, the wave equation (3.5.5) for the vertical velocity *w'* reduces to

$$\left(\frac{\partial}{\partial t} + U\frac{\partial}{\partial x}\right)^2 \frac{\partial^2 w'}{\partial z^2} + N^2\frac{\partial^2 w'}{\partial x^2} = 0. \qquad (3.5.19)$$

In the other limit, $N^2 << \Omega^2$, the buoyancy oscillation period is much greater than that of the disturbance ($2\pi / \omega$) or advection time of the air parcel (*L*/*U*). Therefore, the buoyancy force plays insignificant role in this flow regime. In

this situation, the wave energy is not able to propagate vertically, and the wave disturbance will remain locally in the vicinity of the forcing. The vertical momentum equation, (3.5.2), reduces to

$$\frac{\partial w'}{\partial t} + U\frac{\partial w'}{\partial x} = -\frac{1}{\rho_o}\frac{\partial p'}{\partial z}. \qquad (3.5.20)$$

Thus, only the vertical pressure gradient force contributes to the vertical acceleration. It can also be shown from (3.5.9) that the amplitude of the disturbance decreases exponentially with height. As discussed earlier, this special case is called the *evanescent flow regime*. The wave equation for *w'* reduces to

$$\left(\frac{\partial}{\partial t} + U\frac{\partial}{\partial x}\right)^2\left(\frac{\partial^2 w'}{\partial x^2} + \frac{\partial^2 w'}{\partial z^2}\right) = 0. \qquad (3.5.21)$$

If the flow starts with no relative vorticity in the y-direction (i.e. if $\partial u'/\partial z - \partial w'/\partial x = 0$ at $t = 0$), then the above equation reduces to a two-dimensional form of the Laplace's equation

$$\frac{\partial^2 w'}{\partial x^2} + \frac{\partial^2 w'}{\partial z^2} = 0. \qquad (3.5.22)$$

Because this type of flow is everywhere vorticity-free, it is often referred to as *potential* (*irrotational*) *flow*.

3.6 Inertia-gravity waves

When the Rossby number ($R_o = U/fL$) becomes smaller, rotational effects need to be considered. In this situation, buoyancy and Coriolis forces can act together as restoring forces and inertia-gravity waves can be generated. The governing equations are similar to (3.5.1)-(3.5.4), but with three-dimensional and rotational effects included,

$$\frac{\partial u'}{\partial t} + U\frac{\partial u'}{\partial x} - fv' + \frac{1}{\rho_o}\frac{\partial p'}{\partial x} = 0, \tag{3.6.1}$$

$$\frac{\partial v'}{\partial t} + U\frac{\partial v'}{\partial x} + fu' + \frac{1}{\rho_o}\frac{\partial p'}{\partial y} = 0, \tag{3.6.2}$$

$$\frac{\partial w'}{\partial t} + U\frac{\partial w'}{\partial x} - g\frac{\theta'}{\theta_o} + \frac{1}{\rho_o}\frac{\partial p'}{\partial z} = 0, \tag{3.6.3}$$

$$\frac{\partial u'}{\partial x} + \frac{\partial v'}{\partial y} + \frac{\partial w'}{\partial z} = 0, \tag{3.6.4}$$

$$\frac{\partial \theta'}{\partial t} + U\frac{\partial \theta'}{\partial x} + \frac{N^2\theta_o}{g}w' = 0. \tag{3.6.5}$$

The above set of equations can be combined into a single equation for *w'*,

$$\left(\frac{\partial}{\partial t} + U\frac{\partial}{\partial x}\right)^2\left(\frac{\partial^2 w'}{\partial x^2} + \frac{\partial^2 w'}{\partial y^2} + \frac{\partial^2 w'}{\partial z^2}\right) + f^2\frac{\partial^2 w'}{\partial z^2} + N^2\left(\frac{\partial^2 w'}{\partial x^2} + \frac{\partial^2 w'}{\partial y^2}\right) = 0. \tag{3.6.6}$$

Again, applying the method of normal modes to *w'* in (*x*, *y*, *t*),

$$w' = \hat{w}(z)\, exp\,[i(kx + ly - \omega t)], \tag{3.6.7}$$

and substituting it into (3.6.6) lead to

$$\frac{\partial^2 \hat{w}}{\partial z^2} + \frac{K^2(N^2 - \Omega^2)}{\Omega^2 - f^2}\hat{w} = 0, \tag{3.6.8}$$

where *K* is the horizontal wave number ($= \sqrt{k^2 + l^2}$). Similar to the pure gravity wave solutions, the above equation has solutions of the form,

$$\hat{w} = A e^{imz} + B e^{-imz}, \tag{3.6.9}$$

where *m*, the vertical wave number, is defined as,

$$m^2 = \frac{K^2(N^2 - \Omega^2)}{\Omega^2 - f^2}. \tag{3.6.10}$$

It is clear from (3.6.9) that wave properties depend on the sign of m^2. Based on the signs of the numerator and denominator in (3.6.10) and on typical values of basic state flow parameters observed for waves in both the atmosphere and ocean (*N* is normally greater than *f*), three different flow regimes may be identified. The approximated governing equations and dispersion relations for the different flow regimes are summarized in Table 3.2. Their characteristics are described below.

The first flow regime occurs when $\Omega^2 > N^2 > f^2$. In this flow regime *m* is imaginary, so term A of (3.6.9) decays exponentially with height, while term B increases exponentially with height. The flow behavior is similar to the evanescent waves, as discussed in (3.6.10) for the case of $N^2/\Omega^2 < 1$, except that N^2 is required to be greater than f^2, and is referred to as the *high-frequency evanescent flow regime*.

When $\Omega^2 >> N^2 > f^2$, (3.6.10) reduces to

$$m^2 \approx -K^2. \tag{3.6.11}$$

In this extreme case, both the buoyancy and Coriolis forces play insignificant roles in the process of wave generation and propagation. The governing equation for the vertical velocity *w'* reduces to what is essentially a three-dimensional version of (3.5.21),

$$\left(\frac{\partial}{\partial t}+U\frac{\partial}{\partial x}\right)^2\left(\frac{\partial^2 w'}{\partial x^2}+\frac{\partial^2 w'}{\partial y^2}+\frac{\partial^2 w'}{\partial z^2}\right)=0. \qquad (3.6.12)$$

Thus, this extreme flow regime is characterized by *potential* (*irrotational*) *flow*, as discussed in the previous section. In this extreme case, for a steady state flow, the flow regime criterion becomes $L/U << 2\pi/N < 2\pi/f$. The second flow regime is when $N^2 > \Omega^2 > f^2$. In this flow regime, m is real and the waves are able to propagate freely in the vertical direction. Thus, the flow regime is referred to as the *vertically propagating inertia-gravity wave regime*. The two possible mathematical solutions of (3.6.9) represent either an upward or a downward propagation of energy. If the wave is generated by a low-level source such as stably stratified flow over a mountain, the radiation condition requires that the wave energy propagate away from the energy source, i.e., upward and away from the orographic forcing. This also applies to the boundary condition at $z = +\infty$ for elevated thermal forcing. However, both terms in (3.6.9) must be retained in the heating layer (forcing region) and in the layer between the heating base and the lower boundary (the Earth's surface). Above the forcing, either orographic forcing or elevated latent heating, term A should be retained to allow the energy to propagate upward, as required by the radiation boundary condition (Section 4.4).

Since the ratio *N/f* is typically large in both the atmosphere and the ocean, this flow regime is applicable to a wide range of intrinsic wave frequencies. When $N^2 > \Omega^2 >> f^2$ and $O(N) = O(\Omega)$, (3.6.10) reduces to

$$m^2 \approx K^2\left(\frac{N^2}{\Omega^2}-1\right). \qquad (3.6.13)$$

In this limit, rotational effects may be ignored, and the flow belongs to the *nonrotating* or *pure gravity wave regime*, as described in Section 3.5. Notice that for this extreme case, the flow regime criterion becomes $2\pi / N < L/U << 2\pi / f$ or $U / NL < 1/2\pi << R_o$ for a steady state flow. This implies that in order to generate pure gravity waves, the Rossby number of the basic state flow must be very large, normally much greater than 1. The governing equation for the vertical velocity w' in this extreme case becomes

$$\left(\frac{\partial}{\partial t}+U\frac{\partial}{\partial x}\right)^2\left(\frac{\partial^2 w'}{\partial x^2}+\frac{\partial^2 w'}{\partial y^2}+\frac{\partial^2 w'}{\partial z^2}\right)+N^2\left(\frac{\partial^2 w'}{\partial x^2}+\frac{\partial^2 w'}{\partial y^2}\right)=0. \qquad (3.6.14)$$

When $N^2 >> \Omega^2 >> f^2$, (3.6.10) reduces to

$$m^2 \approx \left(\frac{KN}{\Omega}\right)^2. \qquad (3.6.15)$$

This is identical to the *nonrotating hydrostatic gravity wave regime*, as discussed earlier. The governing equation for w' in this extreme case becomes

$$\left(\frac{\partial}{\partial t}+U\frac{\partial}{\partial x}\right)^2\frac{\partial^2 w'}{\partial z^2}+N^2\left(\frac{\partial^2 w'}{\partial x^2}+\frac{\partial^2 w'}{\partial y^2}\right)=0. \qquad (3.6.16)$$

The flow regime criterion becomes $2\pi / N << L/U << 2\pi / f$ for a steady state flow. This implies that the fluid parcel advection time is much longer than the period of buoyancy oscillation allowing the disturbance to propagate vertically, but much shorter than the inertial oscillation period. In this nonrotating hydrostatic wave regime, only upward propagating waves are allowed.

When $N^2 >> \Omega^2 > f^2$ and $O(\Omega) = O(f)$, (3.6.10) reduces to

$$m^2 \approx \frac{K^2 N^2}{\Omega^2 - f^2}. \qquad (3.6.17)$$

The flow response belongs to the *hydrostatic inertia-gravity wave regime*. Thus, the governing equation for *w'* becomes

$$\left[\left(\frac{\partial}{\partial t} + U\frac{\partial}{\partial x}\right)^2 + f^2\right]\frac{\partial^2 w'}{\partial z^2} + N^2\left(\frac{\partial^2 w'}{\partial x^2} + \frac{\partial^2 w'}{\partial y^2}\right) = 0. \qquad (3.6.18)$$

For a basic flow with $N = 0.01\ \mathrm{s}^{-1}$ and $f = 10^{-4}\mathrm{s}^{-1}$, the horizontal scale of typical hydrostatic inertia-gravity waves is on the order of 100 km.

The third flow regime is when $N^2 > f^2 > \Omega^2$. In this flow regime, *m* is imaginary. Similar to the first flow regime ($\Omega^2 > N^2 > f^2$), disturbances decay exponentially in the vertical away from the wave energy source. However, the wave frequency is low, thus the flow response is referred to as the *low-frequency evanescent flow regime*. When $N^2 > f^2 >> \Omega^2$, inertial accelerations play an insignificant role in wave generation and propagation. The flow response is similar to a *quasi-geostrophic flow*. In this limiting case, (3.6.10) reduces to

$$m^2 \approx \frac{-K^2 N^2}{f^2}. \qquad (3.6.19)$$

In this case, the fluid motion is quasi-horizontal and the governing equation for the vertical velocity *w'* becomes

$$f^2 \frac{\partial^2 w'}{\partial z^2} + N^2 \left(\frac{\partial^2 w'}{\partial x^2} + \frac{\partial^2 w'}{\partial y^2} \right) = 0 . \qquad (3.6.20)$$

The horizontal scale for this type of *quasi-geostrophic flow* is on the order of 1000 km for typical values of $N = 0.01$ s^{-1} and $f = 10^{-4}$ s^{-1}. The Rossby number of the basic state flow in this case is much smaller than 1.

In order to better understand the basic wave dynamics, we consider the case of hydrostatic inertia-gravity waves in a quiescent fluid (U = 0). Substituting $\varphi' = \tilde{\varphi} \exp(kx + ly + mz - \omega t)$, where $\varphi = u, v, w, p,$ or θ, into (3.6.1) - (3.6.5) and using the hydrostatic form of (3.6.3) lead to the following polarization relationships in wave number space,

$$\tilde{u} = \frac{1}{\rho_o} \left(\frac{\omega k + ilf}{\omega^2 - f^2} \right) \tilde{p} ; \qquad \tilde{v} = \frac{1}{\rho_o} \left(\frac{\omega l - ikf}{\omega^2 - f^2} \right) \tilde{p} ;$$

$$\tilde{w} = \frac{-\omega}{\rho_o m} \left(\frac{k^2 + l^2}{\omega^2 - f^2} \right) \tilde{p} ; \quad \tilde{\theta} = \frac{iN^2 \theta_o}{\rho_o g m} \left(\frac{k^2 + l^2}{\omega^2 - f^2} \right) \tilde{p} . \qquad (3.6.21)$$

The above relationships are depicted in Fig. 3.10. In the special case of two-dimensional flow ($\partial / \partial y = 0$ or l = 0), it can be shown that the following solutions satisfy the two-dimensional form of (3.6.6),

$$u' = \tilde{u} \cos(kx + mz - \omega t) ; \quad v' = \left(\frac{f}{\omega} \right) \tilde{u} \sin(kx + mz - \omega t) . \qquad (3.6.22)$$

It can be easily shown from the above equations that the velocity vector associated with a plane inertia-gravity wave rotates anticyclonically with time in the Northern Hemisphere. The projection of the motion on the horizontal plane is an ellipse where ω / f is the ratio between the major and minor axes, as depicted in Fig. 3.10b. The velocity vector

associated with an inertia-gravity wave rotates anticylonically with height for upward energy propagation. The particle motion and phase relationship for a Poincaré wave propagating on the ocean surface is similar to that of a hydrostatic inertia-gravity wave. It can also be shown that the ratio of the vertical to horizontal components of the group velocity vector for a two-dimensional, hydrostatic inertia-gravity wave is given by

$$\left|c_{gz} / c_{gx}\right| = \left|k / m\right| = \sqrt{\omega^2 - f^2} / N . \qquad (3.6.23)$$

Therefore, the wave energy of a hydrostatic inertia-gravity wave propagates more horizontally than that of a pure gravity wave with the same wave frequency.

Occasionally, it is observed that large-scale pressure gradients over the ocean are considerably smaller than those over the continents, which leads to a balance between Coriolis and centrifugal forces. Under this situation, fluid parcels follow circular paths, rotating in an anticyclonic sense in the horizontal plane, and that have an oscillation period of one pendulum day ($2\pi / f$). This type of flow is called an inertial flow or inertial oscillation. The radius (R) of curvature of the oscillation can be shown to be $R = -V / f$, where V is the non-negative horizontal wind speed along the direction tangential to the local velocity in the natural coordinates. The negative sign of R indicates the oscillation is anticyclonic (clockwise). The inertial oscillation has been used to explain the formation of low-level jets over the Great Plains to the east of the US Rocky Mountains (Sec. 10.6).

It can be shown that for this particular example

$$\boldsymbol{c}_g \cdot \boldsymbol{k} = 0 . \qquad (3.6.24)$$

This indicates that the group velocity vector for inertia-gravity waves is perpendicular to both the wave number vector and the phase velocity vector.

3.7 Wave reflection levels

Atmospheric waves may be reflected from the Earth's surface, the surface of a fluid, or the internal interface at density discontinuity. If the atmospheric structure, such as the Brunt-Vaisala frequency (N) and the basic wind velocity (U), varies with height, then gravity waves may be reflected from and/or transmitted through the interface at which rapid changes in atmospheric structure occur.

In order to help understand the basic properties of wave reflection and transmission, we consider a simple fluid system similar to that for pure gravity waves [(3.5.5)], except that the fluid is now comprised of two layers, each with different buoyancy frequencies (N_1 and N_2 in the lower and upper layers, respectively; see Fig. 3.11). We further assume that there is no basic flow ($U = 0$). Under these constraints, the governing equations for the small-amplitude vertical velocities w_1' and w_2' in each layer of this particular two-dimensional fluid system may be written as

$$\frac{\partial^2}{\partial t^2}\left(\frac{\partial^2 w_1'}{\partial x^2}+\frac{\partial^2 w_1'}{\partial z^2}\right)+N_1^2\frac{\partial^2 w_1'}{\partial x^2}=0, \quad 0\le z<H, \tag{3.7.1}$$

$$\frac{\partial^2}{\partial t^2}\left(\frac{\partial^2 w_2'}{\partial x^2}+\frac{\partial^2 w_2'}{\partial z^2}\right)+N_2^2\frac{\partial^2 w_2'}{\partial x^2}=0, \quad H\le z. \tag{3.7.2}$$

Applying the method of normal modes, $w' = \hat{w}(z)\exp[i(kx - \omega t)]$, to the above equations leads to the following equations for the vertical structure in each layer:

$$\frac{\partial^2 \hat{w}_1}{\partial z^2} + m_1^2 \hat{w}_1 = 0, \qquad 0 \le z < H, \qquad (3.7.3)$$

$$\frac{\partial^2 \hat{w}_2}{\partial z^2} + m_2^2 \hat{w}_2 = 0, \qquad H \le z, \qquad (3.7.4)$$

where

$$m_i^2 = k^2\left(N_i^2/\omega^2 - 1\right), \quad i = 1, 2. \qquad (3.7.5)$$

In fact, (3.7.5) represents the dispersion relationships in each layer, which are identical to (3.5.12) if m is replaced by m_i. Note that in the above equation (3.7.5), we have assumed that the wave frequencies and wavelength are identical in both layers. This simple type of piecewise layered model is able to provide the fundamental wave dynamics. It can be shown that the following solutions satisfy (3.7.3) and (3.7.4),

$$\hat{w}_1 = A e^{im_1(z-H)} + B e^{-im_1(z-H)}, \qquad 0 \le z < H \qquad (3.7.6)$$

$$\hat{w}_2 = C e^{im_2(z-H)} + D e^{-im_2(z-H)}, \qquad H \le z. \qquad (3.7.7)$$

Similar to the one-layer theory discussed in the previous section, the flow response is quite different depending on whether m_i (where $i = 1$ or 2) is real or imaginary (i.e. whether $N > \omega$ or $N < \omega$). If we assume a less stable layer sitting on top of a more stable layer ($N_2 < N_1$), then this leads to three possible cases: (a) $N_i > \omega$ for $i = 1, 2$; (b)

$N_i < \omega$ for i=1, 2; or (c) $N_2 < \omega < N_1$ (Fig. 3.11). This type of situation $N_2 < N_1$ may occur in the vicinity of a thunderstorm in which the lower layer is more stable due to the evaporative cooling associated with rainfall. The opposite situation, ($N_2 > N_1$), often occurs when a mixed boundary layer is produced by surface sensible heating during the day, or when the stratosphere is considered in the problem, when N_2 is normally two to three times larger than N_1.

In the following, we will restrict our attention to the case with $N_2 < \omega < N_1$ (i.e. Case ω_2 of Fig. 3.11). Solutions for other cases may be obtained in a similar manner. The lower boundary condition for flow over a flat surface requires that the normal velocity component vanish, i.e. $w' = 0$ at $z = 0$. Applying this lower boundary condition to (3.7.6) yields

$$\hat{w}_1 = B\left[e^{-im_1(z-H)} - e^{2im_1H}e^{im_1(z-H)}\right], \qquad 0 \le z < H\,. \tag{3.7.8}$$

In the above equation, the first term inside the square bracket represents waves with upward energy propagation, while the second term represents waves with downward energy propagation, since $z - H$ is negative. If the wave energy source is located at the surface, then the absolute value of $\exp(2im_1H)$ represents the reflection coefficient. In the upper layer, since m_2 is imaginary, (3.7.7) becomes

$$\hat{w}_2 = C\,e^{-n_2(z-H)} + D\,e^{n_2(z-H)}, \qquad H \le z, \tag{3.7.9}$$

where $n_2 = im_2 = k\sqrt{1 - N_2^2/\omega^2}$ is a real number. For a wave energy source located in the lower layer, the upper boundary condition requires a bounded solution, which, in turn, requires that $D = 0$. Thus, (3.7.7) reduces to

$$\hat{w}_2 = C\, e^{-n_2(z-H)}, \qquad H \le z. \tag{3.7.10}$$

The above equation represents evanescent waves, as described in Section 3.5. However, for cases with real values of m_2, the upper boundary condition is governed by the radiation boundary condition, which will be discussed in Section 4.4. Therefore, the radiation condition requires that $D = 0$ if the wave energy source is located in the lower layer. Coefficients B and C are determined by boundary conditions at the interface, i.e. by imposing the appropriate kinematic and dynamic boundary conditions at $z = H$. The kinematic boundary condition requires that

$$\boldsymbol{V_1} \cdot \boldsymbol{n_1} = \boldsymbol{V_2} \cdot \boldsymbol{n_2}, \tag{3.7.11}$$

where the subscripts indicate the upper or lower layer; $\boldsymbol{V}_i$ is the total velocity in layer i; and $\boldsymbol{n}_i$ is the unit vector normal to the boundary in each layer. Note that $\boldsymbol{n}_i$ in (3.7.11) is a vector, which should not be confused with the n_i used in (3.7.9) and (3.7.10). For a small-amplitude (linear) perturbation, the unit normal vector is almost vertical since the wave amplitude is much smaller than the wavelength. This then implies that

$$w'_1 = w'_2. \tag{3.7.12}$$

Another interface boundary condition is the dynamic boundary condition specifying continuity of pressure at $z = H$, i.e. $p'_1 = p'_2$, which leads to

$$\frac{\partial w'_1}{\partial z} = \frac{\partial w'_2}{\partial z}. \tag{3.7.13}$$

Applying (3.7.12) to (3.7.8) and (3.7.10) at $z = H$ gives

$$\hat{w}_1 = \frac{C}{1-e^{-2im_1H}}\left[e^{im_1(z-H)} - e^{-2im_1H}e^{-im_1(z-H)}\right], \quad 0 \le z < H\,. \tag{3.7.14}$$

Applying the dynamic boundary condition, (3.7.13), to (3.7.14) and (3.7.10) yields the dispersion relationship for this two-layer fluid system,

$$e^{-2im_1H} = \frac{n_2 + im_1}{n_2 - im_1}\,. \tag{3.7.15}$$

This expression may also be used to find the eigenvalues, ω and k, which are needed for substitution into (3.7.15) in order to obtain the eigenfunctions that describe the vertical structure of the wave,

$$\hat{w}_1 = C\left[\left(\frac{m_1 + in_2}{2m_1}\right)e^{im_1(z-H)} + \left(\frac{m_1 - in_2}{2m_1}\right)e^{-im_1(z-H)}\right]. \tag{3.7.16}$$

The reflection coefficient for a forcing located at the surface (z = 0) and the wave being reflected at $z = H$ may be obtained by taking the absolute value of the ratio of the first term (term A) to the second term (term B) inside the square bracket of the above equation, which gives the reflection coefficient $r = \left|(m_1 + in_2)/(m_1 - in_2)\right|$. Note that $z - H$ is negative in the lower layer.

In addition to interfacial discontinuities in stratification, wave reflection may also occur when the vertical profiles of the basic state wind and the stratification (Brunt-Vaisala frequency) vary continuously throughout the fluid (Fig. 3.12). To elucidate this further, we consider a two-dimensional, linear, nonrotating, inviscid, Boussinesq fluid system governed by (3.5.1) - (3.5.4), but whose basic state is generalized, to allow for both the background wind and Brunt-

Vaisala frequency to vary with height. The equation governing this special type of fluid system may also be derived directly from the generalized linear equation set, (2.2.14) - (2.2.18) and is given by

$$\frac{\partial^2 \hat{w}}{\partial z^2} + m^2(z)\hat{w} = 0\,, \tag{3.7.17}$$

where

$$m^2(z) = \frac{N^2}{(U-c)^2} - \frac{U_{zz}}{U-c} - k^2\,,\ c = \frac{\omega}{k}\,. \tag{3.7.18}$$

Equation (3.7.17) is a reduced form in the wave-number space of the *Taylor-Goldstein equation*,

$$\frac{D^2}{Dt^2}\nabla^2 w' - U_{zz}\frac{D}{Dt}\left(\frac{\partial w'}{\partial x}\right) + N^2\frac{\partial^2 w'}{\partial x^2} = 0\,. \tag{3.7.19}$$

Note that m in (3.7.18) can be viewed as the vertical wave number, and the solutions of (3.7.17) can be written in the form of $\exp(\pm imz)$ when U and N are constant. If m^2 changes sign from positive to negative at a certain level, then m will change from a real to an imaginary number. A transition from the vertically propagating wave regime to the evanescent flow regime occurs based on an argument similar to that given for the solutions of (3.5.8) and (3.5.9). If a vertically propagating wave-like disturbance exists below that particular level, such as $z = H$ for ω_2 of Fig. 3.11, it will exponentially decay above that level. In this situation, the wave energy is not able to freely propagate vertically above $z = H$ and is therefore forced to reflect back. This level is called the *wave reflection level*. If such a reflection level exists above the lower, rigid, flat surface, this atmospheric layer then acts as a wave guide in trapping the wave energy between the reflection level and the surface and allows for the wave energy to effectively propagate far downstream

horizontally. One well-known example of gravity wave reflection in the atmosphere is the lee waves (Section 5.2) generated by stratified airflow over a two-dimensional mountain ridge when the stratification (wind speed) is much stronger (smaller) in the lower layer compared to the upper layer. The idea of wave reflection in a slow-varying density gradient or stratification may also be traced by the paths of rays, whose directions (α) are defined locally by (3.5.13), as shown by the long-thin arrows in Fig. 3.12. Ray paths are defined as paths where the tangent at any one point is in the direction of the group velocity (relative to the ground) of the waves. When a group of waves approaches the reflection level where $\omega = N$, α approaches 0, and the wave fronts are turned towards the vertical, reflecting the wave energy.

3.8 Critical levels

Another important phenomenon associated with gravity waves is the change in wave properties across a critical level. A *critical level* (z_c) is defined as the level at which the vertically sheared basic flow $U(z)$ is equal to the horizontal phase speed (c) of the wave or disturbance, i.e. $U(z_c) = c$. Note that the equation governing the vertical structure (3.7.17) has a singularity at the critical level. From an observational analysis of the Oklahoma squall line as depicted in Fig. 6.12 (Chapter 6), there exists a critical level near 6 km. Climatological studies indicate that most midlatitude squall lines exhibit a critical level in the mid-troposphere (Bluestein and Jain 1985; Wyss and Emanuel 1988).

Nonlinear numerical simulations indicate that a high-drag or severe-wind state may be established after the upward propagating wave breaks above the mountain. The wave-breaking region is characterized by strong turbulent mixing with a local wind reversal on top of it. Note that the critical level coincides with the wind reversal level for a stationary mountain wave because the phase speed there is zero. The wave breaking region aloft might act as an internal boundary that reflects the upward propagating waves back to the ground and produces a high-drag state through partial resonance with the upward propagating mountain waves, as will be discussed in Ch. 5. One example of the wave-induced critical level simulated by a numerical model is given in Figs. 5.9 and 5.10 (Chapter 5).

Using an asymptotic method, such as the WKBJ method (e.g., Olver 1997), it is found that an upward propagating internal gravity wave packet in a nonrotating stably stratified fluid would approach the critical level for the dominant frequency and wave number of the packet, but it would not reach the critical level in any finite period of time since along a ray path, $dz/dt \propto (z - z_c)^2$ as $z \to z_c$, which gives $(t - t_o) \propto 1/(z - z_c)$ as $z \to z_c$ (Bretherton 1966). This means that it will take an infinite amount of time for a gravity wave packet to reach the critical level. Thus, the internal wave is physically *absorbed* at the critical level, instead of being either transmitted or reflected, as discussed in the previous section. In the real atmosphere, a gravity wave is composed by a number of different wave modes which propagate at different phase speeds. This will form a layer of critical levels, i.e. a *critical layer*. This particular type of internal wave behavior in a stratified fluid is illustrated in Fig. 3.13. When the wave energy associated with a wave packet propagates toward the critical level, the group velocity becomes more horizontal and eventually is oriented completely horizontally in the vicinity of the critical level. Near the critical level, the phase velocity is oriented

downward since it is itself perpendicular to the group velocity, and fluid parcel motions become horizontal. The vertical wavelength also decreases as the wave packet approaches the critical level. In the following discussion for obtaining the solution for (3.7.17), we will assume that the Richardson number, *Ri* ($= N^2/U_z^2$) is always greater than 1/4. *Ri* is also known as the *gradient Richardson number*.

Near $z = z_c$, $U(z)U(z)$ and $N(z)N(z)$ may be expanded in power series

$$U(z) = c + U_c'(z - z_c) + ...$$

$$N(z) = N_c + N_c'(z - z_c) + ... \qquad (3.8.1)$$

where the prime denotes differentiation with respect to *z* and the subscript "*c*" denotes the function value at the critical level (z_c). We assume that z_c is a *regular singularity*, which requires $U'(z_c) \neq 0$. Hence, we seek a solution for (3.7.17) of the form,

$$\hat{w}(z) = \sum_{n=0}^{\infty} a_n (z - z_c)^{n+\alpha}, \quad a_o \neq 0, \; n \text{ is an integer.} \qquad (3.8.2)$$

Substituting the above expression into the Taylor-Goldstein equation, (3.7.17), leads to the indicial equation,

$$\alpha^2 - \alpha + Ri_c = 0 \qquad (3.8.3)$$

where $Ri_c = \left(N_c / U_c'\right)^2$. The above indicial equation has the following solutions,

$$\alpha = 1/2 \pm i\mu; \quad \mu = \sqrt{Ri_c - 1/4} \qquad (3.8.4)$$

Thus, near $z = z_c$, a series solution may be found,

$$\hat{w}(z) \approx A(z-z_c)^{1/2+i\mu} + B(z-z_c)^{1/2-i\mu}$$
$$= A\ \exp\Big[\big(1/2+i\mu\big)\big(\ln|z-z_c|+i\ \arg(z\text{-}z_c)\big)\Big] + B\exp\Big[\big(1/2-i\mu\big)\big(\ln|z-z_c|+i\ \arg(z\text{-}z_c)\big)\Big] \qquad (3.8.5)$$

where "arg" denotes the argument of a complex number. Both $\hat{w}_A$ and $\hat{w}_B$ (i.e., terms in (3.8.5) with coefficients A and B, respectively) have a branch point at $z = z_c$. In other words, both $\hat{w}_A$ and $\hat{w}_B$ are not single-valued functions when one winds a circle counterclockwise once around z_c. For the sake of definiteness, we may choose that branch of the natural logarithm (ln) function for which $\arg(z-z_c) = 0$ when $z > z_c$ and introduce the branch cut from $z = z_c$ along the negative *x*-axis. Therefore, we obtain

$$\hat{w}_A^+(z) = A\sqrt{|z\text{-}z_c|}\exp[i\mu \ln(z-z_c)],\ \text{and}$$

$$\hat{w}_B^+(z) = B\sqrt{|z\text{-}z_c|}\exp[-i\mu \ln(z-z_c)],\quad \text{for}\quad z > z_c. \qquad (3.8.6)$$

In order to determine the appropriate argument, a small Rayleigh friction term to the *x*-momentum equation (3.5.1) and a small Newtonian cooling term can be added to the thermodynamic energy equation (3.5.4). This gives $\arg(z-z_c) = -\pi\,\mathrm{sgn}(U_c')$ when $z < z_c$. Substituting the above expression into (3.8.5) yields

$$\hat{w}_A^- = A\sqrt{|z\text{-}z_c|}\exp\Big[i\mu\ \ln|z-z_c| - (1/2)\pi i\ \ \mathrm{sgn}\ U_c' + \mu\pi\ \mathrm{sgn}\ U_c'\Big],$$

$$\hat{w}_B^- = B\sqrt{|z\text{-}z_c|}\exp\Big[-i\mu\ \ln|z-z_c| - (1/2)\pi i\ \ \mathrm{sgn}\ U_c' - \mu\pi\ \mathrm{sgn}\ U_c'\Big],\ \text{for}\ z < z_c. \qquad (3.8.7)$$

Both solutions $\hat{w}_A$ and $\hat{w}_B$ in (3.8.6) and (3.8.7) satisfy (3.7.17) mathematically; however, they have different physical meanings and need to be properly determined. From (3.8.6) and (3.8.7), we have

$$\left|\frac{\hat{w}_A^+}{\hat{w}_A^-}\right| = \exp(-\mu\pi \ \text{sgn} \ U_c'); \qquad \left|\frac{\hat{w}_B^+}{\hat{w}_B^-}\right| = \exp(\mu\pi \ \text{sgn} \ U_c'). \tag{3.8.8}$$

For $U_c' > 0$ and low-level forcing, the amplitude of the disturbance generated in the lower layer should decrease as it passes across the critical level into the upper layer. Thus, we must choose $\hat{w}_A$. The proper solution can be found for other situations as well. Note that the above equation also indicates that the wave energy is exponentially attenuated through the critical level (Booker and Bretherton 1967). As mentioned earlier, the vertical wave number increases, and the perturbation velocity becomes increasingly horizontal as one approaches the critical level, because

$$m^2(z) \approx \frac{N^2}{(U-c)^2}. \tag{3.8.9}$$

This implies that $m \to \infty$ as $z \to z_c$. Thus, the vertical wavelength approaches zero near the critical level. This property is also depicted by Fig. 3.13. In the real atmosphere, a localized disturbance is often composed of many Fourier wave components, each with a different wavelength. Since each Fourier wave component has its own critical level, where $U = c = \omega/k$, an atmospheric layer of finite thickness composed of these critical levels, referred to as the critical layer, is often associated with a localized disturbance.

The flow near a critical level is highly nonlinear, since a small perturbation in the horizontal velocity field will necessarily exceed the basic horizontal flow velocity in the vicinity of the critical level, in a reference frame moving

with the phase speed of the wave. Thus, linear theories are not accurate in the vicinity of a critical level. Based on numerical simulations of varying the Richardson number, three flow regimes have been found (Breeding 1971). For $Ri > 2.0$, the interaction between the incident wave and the mean flow is largely similar to that predicted by the linear theory as outlined above. That is, very little of the incident wave energy penetrates through the critical level. For $0.25 < Ri < 2.0$, a significant amount of the wave energy is reflected, part of which can be predicted by linear theory. This condition represents a balance between the outward diffusion of the added momentum from the incident wave and the rate at which it is absorbed at the critical level. When *Ri* falls into this range, some wave energy is also transmitted through the critical level. For $Ri < 0.25$, wave overreflection is predicted. Note that these regime boundaries could be more accurately defined with more recent and sophisticated numerical models. When *wave overreflection* occurs, more energy than that associated with the incident wave is reflected back from the critical level, because the flow possesses shear instability (Lindzen and Rosenthal 1983). In this situation, the wave is able to extract energy and momentum from the basic flow during the reflection process. If the overreflected waves are in phase with the incident waves, waves may grow exponentially with time by resonance, i.e. the *normal mode instability* exists. If the overreflected waves are partially in phase with the incident waves, waves may grow algebraically with time by partial resonance, i.e., the *algebraic mode instability* exists. Under certain conditions, such as an unstable layer containing a critical level and capping a stable layer, a wave duct can exist for mesoscale gravity waves, and wave absorption, transmission, and overreflection may occur at different ranges of *Ri* (see Fig. 4.13 and relevant discussions).

Figure 3.14 shows the linear, steady state responses to a prescribed heating in the layer below the critical level ($z_c = 0$) of a stably stratified flow with $Ri = 10$ and $Ri = 1$. Again, for steady state flow, the critical level coincides with the wind reversal level ($U = 0$). Upward motion is induced in the vicinity of the heat source, while two regions of very weak compensated downdrafts are produced upstream and downstream from the heat source. For the case with $Ri = 10$ (Fig. 3.14a), the flow above the critical level is almost undisturbed due to the exponential attenuation associated with critical level absorption. With $Ri = 1$ (Fig. 3.14b), upstream of the heat source is occupied by subsidence, while downstream of the heat source is occupied by ascending motion. This subsidence occurs due to strong advection (Section 6.2). The disturbance above the critical level is more pronounced because more energy is transmitted through the critical level into the upper layer.

The critical level dynamics can be extended to a rotating fluid flow. In a rotating fluid system, the governing equation for the small-amplitude vertical velocity $w'(t,x,z)$ for a two-dimensional, inviscid, Boussinesq flow on an f plane, can be derived (e.g., Smith 1986) and is given by

$$\frac{D}{Dt}\left(\frac{D^2}{Dt^2}\nabla^2 w' + f^2\frac{\partial^2 w'}{\partial z^2} - U_{zz}\frac{D}{Dt}\frac{\partial w'}{\partial x} + N^2\frac{\partial^2 w'}{\partial x^2}\right) - 2f^2 U_z\frac{\partial^2 w'}{\partial x \partial z} = 0. \qquad (3.8.10)$$

Taking a normal mode approach, substitution of $w' = \hat{w}(z)\exp[ik(x-ct)]$, leads to the following vertical structure equation:

$$\frac{\partial^2 \hat{w}}{\partial z^2} - \frac{2f^2 U_z}{(U-c)[k^2(U-c)^2 - f^2]}\frac{\partial \hat{w}}{\partial z} + \frac{k^2[N^2 - k^2(U-c)^2]}{k^2(U-c)^2 - f^2}\hat{w} = 0. \qquad (3.8.11)$$

The above equation indicates that in addition to the singularity at $U = c$, there are two additional singularities, $U = c \pm f / k$. These additional levels are called *inertial critical levels* (Jones 1967). For incident monochromatic (single wavelength) waves, the inertial critical levels can absorb wave energy in linear flow but tend to reflect wave energy in nonlinear flow (Wurtele *et al*. 1996). Based on the Richardson number ($Ri = N^2 / U_z^2$) and the Rossby number ($R_o = U / fa$, where a is the mountain scale, such as the half-width of a bell-shaped mountain), four flow regimes for two-dimensional back-sheared flow over an isolated mountain ridge on an *f*-plane can be identified: (I) inertia-gravity wave regime, (II) mixed inertia-gravity waves and trapped baroclinic lee wave regime, (III) mixed evanescent wave and trapped baroclinic lee wave regime, and (IV) transient wave regime with possible nongeostrophic baroclinic instability (Shen and Lin 1999). The baroclinic lee wave theory of lee cyclogenesis (Section 5.5) belongs to regime II of moderate R_o and moderate Ri (~ 6.25), or small R_o ($\sim 0.4 - 0.8$) and moderate (large) Ri (≥ 25). It is also found that three-dimensionality, directional wind shear, and rotation promote horizontal energy dispersion (Shutts 2003).

Appendix 3.1 Derivations of shallow-water equations

Consider a non-rotating, hydrostatic, two-layer fluid system with constant densities ρ_1 and ρ_o in the upper and lower layers, respectively, and assume that $\rho_1 < \rho_o$. Note that the horizontal pressure gradients, $\partial p / \partial x$ and $\partial p / \partial y$, are independent of height in each layer if the fluid system is in hydrostatic balance because

$$\frac{\partial}{\partial z}\left(\frac{\partial p}{\partial x}\right)=\frac{\partial}{\partial x}\left(\frac{\partial p}{\partial z}\right)=-\frac{\partial}{\partial x}(\rho g)=0\,, \qquad \text{(A3.1.1)}$$

because the density is constant in each layer. We also assume that no horizontal pressure gradients exist in the upper layer. At point A in Fig. 3.2, we have

$$\frac{p-(p+\delta p_1)}{\delta z}=-\rho_1 g\,, \qquad \text{(A3.1.2)}$$

according to the hydrostatic equation. The above equation leads to

$$p+\delta p_1 = p+\rho_1 g\delta z = p+\rho_1 g\frac{\partial(H+h')}{\partial x}\delta x\,, \qquad \text{(A3.1.3)}$$

where H is the undisturbed upstream fluid depth and h' the perturbation or the vertical displacement from H, and $\partial(H+h')/\partial x$ is the slope of the interface. Similarly, we may derive the pressure at point B,

$$p+\delta p_2 = p+\rho_o g\delta z = p+\rho_o g\frac{\partial(H+h')}{\partial x}\delta x\,. \qquad \text{(A3.1.4)}$$

Thus, the horizontal pressure gradient in the x-direction, $\partial p/\partial x$, at the interface can be approximated by

$$\frac{\partial p}{\partial x}=g\Delta\rho\frac{\partial(h+h_s)}{\partial x}, \qquad \text{(A3.1.5)}$$

where $\Delta\rho=\rho_o-\rho_1$. In deriving (A3.1.5), we have used $h+h_s=H+h'$, where h is the instantaneous depth of the fluid, and h_S is the height of the bottom topography (Fig. 3.2). Similarly, we may derive the horizontal pressure gradient in the y-direction

$$\frac{\partial p}{\partial y} = g\Delta\rho \frac{\partial (h + h_s)}{\partial y}. \qquad \text{(A3.1.6)}$$

Therefore, the horizontal momentum equations become

$$\frac{\partial u}{\partial t} + u\frac{\partial u}{\partial x} + v\frac{\partial u}{\partial y} + w\frac{\partial u}{\partial z} = -g'\frac{\partial (h + h_s)}{\partial x}, \qquad \text{(A3.1.7)}$$

$$\frac{\partial v}{\partial t} + u\frac{\partial v}{\partial x} + v\frac{\partial v}{\partial y} + w\frac{\partial v}{\partial z} = -g'\frac{\partial (h + h_s)}{\partial y}, \qquad \text{(A3.1.8)}$$

where $g' = g\Delta\rho / \rho_o$ is called *reduced gravity*. Assuming that initially there is no vertical shear of the horizontal wind velocity ($\partial u / \partial z = \partial v / \partial z = 0$), it can be shown that *u* and *v* will be independent of *z* at any subsequent time. Under this constraint, (A3.1.7) and (A3.1.8) reduce to

$$\frac{\partial u}{\partial t} + u\frac{\partial u}{\partial x} + v\frac{\partial u}{\partial y} = -g'\frac{\partial (h + h_s)}{\partial x}, \qquad \text{(A3.1.9)}$$

$$\frac{\partial v}{\partial t} + u\frac{\partial v}{\partial x} + v\frac{\partial v}{\partial y} = -g'\frac{\partial (h + h_s)}{\partial y}. \qquad \text{(A3.1.10)}$$

The above equations give (3.4.1) and (3.4.2) respectively.

Integrating the continuity equation, (2.2.4), from the surface of the bottom topography ($z = h_s$) to the interface ($z = h + h_s = H + h'$) with respect to *z* leads to

$$\int_{h_s}^{H+h'} \left(\frac{\partial u}{\partial x} + \frac{\partial v}{\partial y} \right) dz + \int_{h_s}^{H+h'} \frac{\partial w}{\partial z}\, dz = 0, \qquad \text{(A3.1.11)}$$

because $D\rho / Dt = 0$ in each layer of the fluid. Since *u* and *v* are assumed to be independent of *z* initially, then both $\partial u / \partial x$ and $\partial v / \partial y$ will be independent of *z* for all time afterwards. Thus, the vertically integrated mass continuity equation, (A3.1.11), reduces to

$$h\left(\frac{\partial u}{\partial x}+\frac{\partial v}{\partial y}\right)+w(z=h+h_s)-w(z=h_s)=0\,. \qquad \text{(A3.1.12)}$$

The vertical velocity is just the rate at which the height is changing: $w = Dz/Dt = \partial h/\partial t + u\partial h/\partial x + v\partial h/\partial y$. Substituting *w* into (A3.1.12) leads to

$$h\left(\frac{\partial u}{\partial x}+\frac{\partial v}{\partial y}\right)+\left(\frac{\partial\left(h+h_s\right)}{\partial t}+u\frac{\partial\left(h+h_s\right)}{\partial x}+v\frac{\partial\left(h+h_s\right)}{\partial y}\right)-\left(u\frac{\partial h_s}{\partial x}+v\frac{\partial h_s}{\partial y}\right)=0. \quad \text{(A3.1.13)}$$

This can be further reduced to the expression

$$\frac{\partial h}{\partial t}+u\frac{\partial h}{\partial x}+v\frac{\partial h}{\partial y}+h\left(\frac{\partial u}{\partial x}+\frac{\partial v}{\partial y}\right)=0 \qquad \text{(A3.1.14)}$$

because h_s, the height of the bottom topography, is generally assumed to be independent of time. Equation (A3.1.14) gives (3.4.3).

References

Baines, P. G., 1995: *Topographic Effects in Stratified Flows.* Cambridge University Press, 482pp.

Bluestein, H. B., and M. H. Jain, 1985: Formation of mesoscale lines of precipitation: Severe squall lines in Oklahoma during the spring. *J. Atmos. Sci.*, **42**, 1711-1732.

Booker, J. R., and F. P. Bretherton, 1967: The critical layer for internal gravity waves in a shear flow. *J. Fluid Mech.*, **27**, 513-539.

Breeding, R. J., 1971: A nonlinear investigation of critical levels for internal atmospheric gravity waves. *J. Fluid Mech.*, **50**, 545-563.

Bretherton, F. P., 1966: The propagation of groups of internal gravity waves in a shear flow. *Quart. J. Roy. Meteor. Soc.*, **92**, 466-480.

Durran, D. R., 1990: Mountain waves and downslope winds. *Atmospheric Processes over Complex Terrain*, Meteor. Monogr., No. **45**, Amer. Meteor. Soc., 59-81.

Emanuel, K., and D. J. Raymond, 1984: *Dynamics of Mesoscale Weather Systems*. Ed. J. B. Klemp, NCAR, 1984.

Hooke, 1986: Gravity waves, in *Mesoscale Meteorology and Forecasting* (P.S. Ray, Ed.), Boston, Amer. Meteor. Soc., 272-288.

Houghton, D. D., and A. Kasahara, 1968: Non-linear shallow fluid flow over an isolated ridge. Comm. *Pure Appl. Math.*, **21**, 1-23.

Jones, W. L., 1967: Propagation of internal gravity wave in fluids with shear and rotation. *J. Fluid Mech.*, **30**, 439-448.

Klemp, J. B., and D. K. Lilly, 1975: The dynamics of wave-induced downslope winds. *J. Atmos. Sci.*, **32**, 320-339.

Lin, Y.-L., 1987: Two-dimensional response of a stably stratified flow to diabatic heating. *J. Atmos. Sci.*, **44**, 1375-1393.

Lindzen, R. S., and A. J. Rosenthal, 1983: Instabilities in a stratified fluid having one critical level. Part III: Kelvin-Helmholtz instabilities as overreflected waves. *J. Atmos. Sci.*, **40**, 530-542.

Long, R. R., 1970: Blocking effects in flow over obstacles. *Tellus*, **22**, 471-480.

Mowbray, D. E., and B. S. H. Rarity, 1967: A theoretical and experimental investigation of the phase configuration of internal waves of small amplitude in a density stratified liquid. *J. Fluid Mech.*, **28**, 1-16.

Nicholls, M. E., and R. A. Pielke Sr., 2000: Thermally induced compression waves and gravity waves generated by convective storms. *J. Atmos. Sci.*, **57**, 3251-3271.

Olver, F. W. J., 1997: *Asymptotics and Special Functions*. A. K. Peters, Ltd., 592pp.

Shen, B.-W., and Y.-L. Lin, 1999: Effects of critical levels on two-dimensional back-sheared flow over an isolated mountain ridge on an f plane. *J. Atmos. Sci.*, **56**, 3286-3302.

Shutts, G., 2003: Inertia-gravity wave and neutral Eady wave trains forced by directionally sheared flow over isolated hills. *J. Atmos. Sci.*, **60**, 593-606.

Smith, R. B., 1979: The influence of mountains on the atmosphere. *Adv. in Geophys*., **21**, Ed. B. Saltzman, Academic Press, NY, 87-230.

Smith, R. B., 1986: Further development of a theory of lee cyclogenesis. *J. Atmos. Sci.*, **43**, 1582-1602.

Sommerfeld, A., 1949: *Partial Differential Equations in Physics*. Academic Press, 335pp.

Turner, J. S., 1973 *Buoyancy Effects in Fluids*. Cambridge University Press, 368 pp.

Wurtele, M. G., A. Data, and R. D. Sharman, 1996: The propagation of gravity-inertia waves and lee waves under a critical level. *J. Atmos. Sci.*, **53**, 1505-1523.

Wyss, J. and K. A. Emanuel, 1988: The pre-storm environment of midlatitude prefrontal squall lines. *Mon. Wea. Rev.*, **116**, 790–794.

Problems

3.1 Using the normal mode approach, derive the Lamb wave solution from (3.3.1), (3.3.2), (3.3.7) and (3.3.8).

3.2 (a) Derive (3.4.10) from (3.4.7)-(3.4.9). (b) Find the dispersion relation for linear, three-dimensional (x, y, t) shallow water waves. Are the waves dispersive or not? (c) From (b), find the group velocities, c_{gx} and c_{gy}.

3.3 Consider a two-dimensional, one-layer fluid flow over an obstacle. Estimate the Froude number (F) and nondimensional mountain height (M), assuming H = 1000 m, U = 4 ms^{-1}, h_m = 200 m. What is the flow regime, based on the flow regime diagram for one-layer shallow-water system (Fig. 3.3)? Change flow and/or orographic parameters to shift the above flow regime to the other four flow regimes.

3.4 Show that in the flow regime with $N^2 >> \Omega^2$ the vertical momentum equation reduces to the hydrostatic equation, (3.5.18). Show that the vertical wavelength is $2\pi U/N$ for a steady state flow.

3.5 (a) Assuming $N^2 << \Omega^2$, prove that the vertical momentum equation, (3.5.2), reduces to (3.5.20).

(b) Show that (3.5.21) reduces to (3.5.22) for a flow starting with no vorticity at t = 0 (i.e. assume that the flow is initially irrotational).

3.6 Derive (3.6.6) from (3.6.1)-(3.6.5).

3.7 Consider a uniform basic flow, which has a uniform buoyancy frequency N = 0.012 s^{-1}, passing over a mountain with a horizontal scale of 20 km. What is the critical basic flow speed that separates the upward propagating waves and evanescent waves, assuming the Earth's rotation can be ignored?

3.8 (a) Derive the group velocities for inertia-gravity waves for $U = 0$.

(b) Derive (3.6.23) for the ratio of c_{gz} / c_{gx}.

3.9 Derive the dynamic interface boundary condition (3.7.13).

3.10 Derive (3.7.17) from (2.2.14)-(2.2.18) by assuming a two-dimensional ($\partial / \partial y = 0, V = 0$), nonrotating, adiabatic, and Boussinesq flow.

Table captions

Table 3.1: A summary of atmospheric waves

Table 3.2: Dispersion relations and approximated equations of *w'* for mesoscale waves in different flow regimes

Figure captions

Fig. 3.1: Propagation of a wave group and an individual wave. The solid and dashed lines denote the group velocity (c_g) and phase velocity (c_p), respectively. Shaded oval denotes the concentration of wave energy which propagates with the group velocity. The phase speed c_p equals x_i / t_i, where i = 1, 2, or 3. (Adapted after Holton 2004)

Fig. 3.2: A two-layer system of homogeneous fluids. Symbols H, h, h_s, and h' denote the undisturbed fluid depth, actual fluid depth, bottom topography, and perturbation (vertical displacement) from the undisturbed fluid depth, respectively. The densities of the upper and lower layers are ρ_1 and ρ_o, respectively. The pressure perturbations at A and B from p in the upper layer are denoted by $p + \delta p_1$ and $p + \delta p_2$, respectively.

Fig. 3.3: Five flow regimes of the transient one-layer shallow water system, based on the two nondimensional control parameters ($F = U / \sqrt{gH}$, $M = h_m / H$). (a) Regime A: supercritical flow, (b) Regime B: flow with both upstream and downstream propagating hydraulic jump, (c) Regime C: flow with upstream propagating jump and downstream stationary jump, (d) Regime D: completely blocked flow, and (e) Regime E: subcritical flow. The dashed lines in (b) and (c) denote transient water surface. In regimes B and C, upstream flow is partially blocked. (Adapted after Baines 1995 and Durran 1990)

Fig. 3.4: (a) Analysis of potential temperature from aircraft flight data and rawinsondes for the 11 January 1972 Boulder windstorm. The bold dashed line separates data taken from the Queen Air aircraft (before 2200 UTC) and from the Saberliner aircraft (after 0000 UTC) (Adapted after Klemp and Lilly 1975). The severe downslope wind reached a speed greater than 60 ms^{-1}. (b) A sketch of flow Regime C of Fig. 3.3(c), which may be used to explain the phenomenon associated with (a). Q is the volume flux per unit width. (Adapted after Turner 1973)

Fig. 3.5: An internal hydraulic jump associated with a severe downslope windstorm formed along the eastern Sierra Nevada (to the right) and Owens Valley, California. The hydraulic jump was made visible by the formation of clouds and by dust raised from the ground in the turbulent flow behind the jump. (Photographed by Robert Symons)

Fig. 3.6: The evolution of an initial symmetric wave, which is imagined to be composed of three rectangular blocks with shorter blocks on top of longer blocks. The wave speeds of these fluid blocks are approximately equal to $c_n = \sqrt{g(H + nh)}$, based on shallow-water theory, where n = 1, 2, and 3, H is the shallow-water layer depth, and h is the height of an individual fluid block. The wave steepening in (b) and wave overturning in (c) are interpreted by the different wave speeds of different fluid blocks because $c_3 > c_2 > c_1$.

Fig. 3.7: Vertical oscillation of an air parcel in a stably stratified atmosphere when the Brunt-Vaisala frequency is N. The oscillation period of the air parcel is $\tau_b = 2\pi / N$ and the volume of the air parcel is proportional to the area of the circle. (Adapted after Hooke 1986)

Fig. 3.8: (a) Vertically propagating waves and (b) evanescent waves for a linear, two-dimensional, inviscid flow over sinusoidal topography. (Adapted after Smith 1979)

Fig. 3.9: Basic properties of a vertically propagating gravity wave with $k > 0, m < 0,$ and $\omega > 0$. The energy of the wave group propagates with the group velocity ($\boldsymbol{c_g}$, thick blunt arrow), while the phase of the wave propagates with the phase speed ($\boldsymbol{c_p}$). Relations between w', u', p', and θ' as expressed by (3.5.16) and (3.5.17) are also sketched. Symbols H and L denote the perturbation high and low pressures, respectively, while W and C denote the warmest

and coldest regions, respectively, for the wave at t_1. Symbol α defined in (3.5.13) represents the angle of the wave number vector $\boldsymbol{k}$ from the horizontal axis or the wave front (line of constant phase) from the vertical axis. (Adapted after Hooke 1986)

Fig. 3.10: (a) Similar to Fig. 3.9, except for a hydrostatic inertia-gravity wave with $m < 0$, $k > 0$, $l = 0$, $\omega > 0$, and $f > 0$. Meridional (i.e. north-south) perturbation wind velocities (v') are shown by arrows pointed into and out of the page. (b) The projection of fluid particle motion associated with a hydrostatic inertia-gravity wave onto the horizontal plane is an ellipse with ω/f as the ratio of major and minor axes. The velocity vector associated with a plane inertia-gravity wave rotates anticyclonically in the Northern Hemisphere with height for upward energy propagation. (Adapted after Hooke 1986)

Fig. 3.11: Examples of wave reflection in a stratified flow with a piecewise constant profile in Brunt-Vaisala frequency (N). Case ω_1 has wave solutions in both layers; Case ω_2 (wave reflection case) has wave solutions in the lower layer, evanescent solutions in upper layer; and Case ω_3 has evanescent solutions in both layers.

Fig. 3.12: Wave reflection in a continuously stratified fluid. N and T are the Brunt-Vaisala frequency and temperature of the sounding, respectively, and ω is the wave frequency. Ray paths are reflected at the reflection level at which $\omega = N$. A wave packet is also depicted in the figure. The short blunt arrows and long thin arrows denote the group and phase velocities, respectively, of the wave packet. Particle motions are parallel to the constant phase lines or wave fronts, which become vertically oriented at the reflection level since α, defined in (3.5.13) and also illustrated in Fig. 3.9, approaches 0. (Adapted after Hooke 1986)

Fig. 3.13: The propagation of a wave packet upward toward a critical level located at $z = z_c$. The particle motions are parallel to the wave crests, which are denoted by straight lines. Note that the vertical wavelength decreases as the wave packet approaches the critical level. The phase lines are horizontally oriented at the critical level in this case. (Adapted after Bretherton 1966)

Fig. 3.14: (a) Streamlines for a linear, steady-state stratified airflow over an isolated heat source. The concentrated heating region is shaded. The basic flow has a linear shear (U_z = constant) and its Richardson number (Ri) is 10. (b) Same as (a) except for $Ri = 1$. All contour values are nondimensionalized. The streamfunction (ψ) used for constructing the streamlines is defined as $u = \partial\psi / \partial z$ and $w = -\partial\psi / \partial x$. (After Lin 1987)

Figure captions

Fig. 3.1: Propagation of a wave group and an individual wave. The solid and dashed lines denote the group velocity (c_g) and phase velocity (c_p), respectively. Shaded oval denotes the concentration of wave energy which propagates with the group velocity. The phase speed c_p equals x_i / t_i, where i = 1, 2, or 3. (Adapted after Holton 2004)

Fig. 3.2: A two-layer system of homogeneous fluids. Symbols H, h, h_s, and h' denote the undisturbed fluid depth, actual fluid depth, bottom topography, and perturbation (vertical displacement) from the undisturbed fluid depth, respectively. The densities of the upper and lower layers are ρ_1 and ρ_o, respectively. The pressure perturbations at A and B from p in the upper layer are denoted by $p + \delta p_1$ and $p + \delta p_2$, respectively.

Fig. 3.3: Five flow regimes of the transient one-layer shallow water system, based on the two nondimensional control parameters ($F = U / \sqrt{gH}$, $M = h_m / H$). (a) Regime A: supercritical flow, (b) Regime B: flow with both upstream and downstream propagating hydraulic jump, (c) Regime C: flow with upstream propagating jump and downstream stationary jump, (d) Regime D: completely blocked flow, and (e) Regime E: subcritical flow. The dashed lines in (b) and (c) denote transient water surface. In regimes B and C, upstream flow is partially blocked. (Adapted after Baines 1995 and Durran 1990)

Fig. 3.4: (a) Analysis of potential temperature from aircraft flight data and rawinsondes for the 11 January 1972 Boulder windstorm. The bold dashed line separates data taken from the Queen Air aircraft (before 2200 UTC) and from the Saberliner aircraft (after 0000 UTC) (Adapted after Klemp and Lilly 1975). The severe downslope wind

reached a speed greater than 60 ms^{-1}. (b) A sketch of flow Regime C of Fig. 3.3(c), which may be used to explain the phenomenon associated with (a). Q is the volume flux per unit width. (Adapted after Turner 1973)

Fig. 3.5: An internal hydraulic jump associated with a severe downslope windstorm formed along the eastern Sierra Nevada (to the right) and Owens Valley, California. The hydraulic jump was made visible by the formation of clouds and by dust raised from the ground in the turbulent flow behind the jump. (Photographed by Robert Symons)

Fig. 3.6: The evolution of an initial symmetric wave, which is imagined to be composed of three rectangular blocks with shorter blocks on top of longer blocks. The wave speeds of these fluid blocks are approximately equal to $c_n = \sqrt{g(H+nh)}$, based on shallow-water theory, where n = 1, 2, and 3, H is the shallow-water layer depth, and h is the height of an individual fluid block. The wave steepening in (b) and wave overturning in (c) are interpreted by the different wave speeds of different fluid blocks because $c_3 > c_2 > c_1$.

Fig. 3.7: Vertical oscillation of an air parcel in a stably stratified atmosphere when the Brunt-Vaisala frequency is N. The oscillation period of the air parcel is $\tau_b = 2\pi / N$ and the volume of the air parcel is proportional to the area of the circle. (Adapted after Hooke 1986)

Fig. 3.8: (a) Vertically propagating waves and (b) evanescent waves for a linear, two-dimensional, inviscid flow over sinusoidal topography.

Fig. 3.9: Basic properties of a vertically propagating gravity wave with $k > 0, m < 0,$ and $\omega > 0$. The energy of the wave group propagates with the group velocity ($\boldsymbol{c_g}$, thick blunt arrow), while the phase of the wave propagates with

the phase speed ($\boldsymbol{c}_p$). Relations between *w', u', p',* and θ' as expressed by (3.5.16) and (3.5.17) are also sketched. Symbols H and L denote the perturbation high and low pressures, respectively, while W and C denote the warmest and coldest regions, respectively, for the wave at t_1. Symbol α defined in (3.5.13) represents the angle of the wave number vector $\boldsymbol{k}$ from the horizontal axis or the wave front (line of constant phase) from the vertical axis. (Adapted after Hooke 1986)

Fig. 3.10: (a) Similar to Fig. 3.9, except for a hydrostatic inertia-gravity wave with $m < 0$, $k > 0$, $l = 0$, $\omega > 0$, and $f > 0$. Meridional (i.e. north-south) perturbation wind velocities (v') are shown by arrows pointed into and out of the page. (b) The projection of fluid particle motion associated with a hydrostatic inertia-gravity wave onto the horizontal plane is an ellipse with ω/f as the ratio of major and minor axes. The velocity vector associated with a plane inertia-gravity wave rotates anticyclonically in the Northern Hemisphere with height for upward energy propagation. (Adapted after Hooke 1986)

Fig. 3.11: Examples of wave reflection in a stratified flow with a piecewise constant profile in Brunt-Vaisala frequency (N). Case ω_1 has wave solutions in both layers; Case ω_2 has wave solutions in the lower layer, evanescent solutions in upper layer; and Case ω_3 has evanescent solutions in both layers. The forcing is assumed at $z = 0$.

Fig. 3.12: Wave reflection in a continuously stratified fluid. N and T are the Brunt-Vaisala frequency and temperature of the sounding, respectively, and ω is the wave frequency. Ray paths are reflected at the reflection level at which $\omega = N$. A wave packet is also depicted in the figure. The short blunt arrows and long thin arrows denote the group and phase velocities, respectively, of the wave packet. Particle motions are parallel to the constant phase lines or

wave fronts, which become vertically oriented at the reflection level since α, defined in (3.5.13) and also illustrated in Fig. 3.9, approaches 0. (Adapted after Hooke 1986)

Fig. 3.13: The propagation of a wave packet upward toward a critical level located at $z = z_c$. The particle motions are parallel to the wave crests, which are denoted by straight lines. Note that the vertical wavelength decreases as the wave packet approaches the critical level. The phase lines are horizontally oriented at the critical level in this case. (Adapted after Bretherton 1966)

Fig. 3.14: (a) Streamlines for a linear, steady-state stratified airflow over an isolated heat source. The concentrated heating region is shaded. The basic flow has a linear shear (U_z = constant) and its Richardson number (Ri) is 10. (b) Same as (a) except for $Ri = 1$. All contour values are nondimensionalized. The streamfunction (ψ) used for constructing the streamlines is defined as $u = \partial\psi / \partial z$ and $w = -\partial\psi / \partial x$. (After Lin 1987)

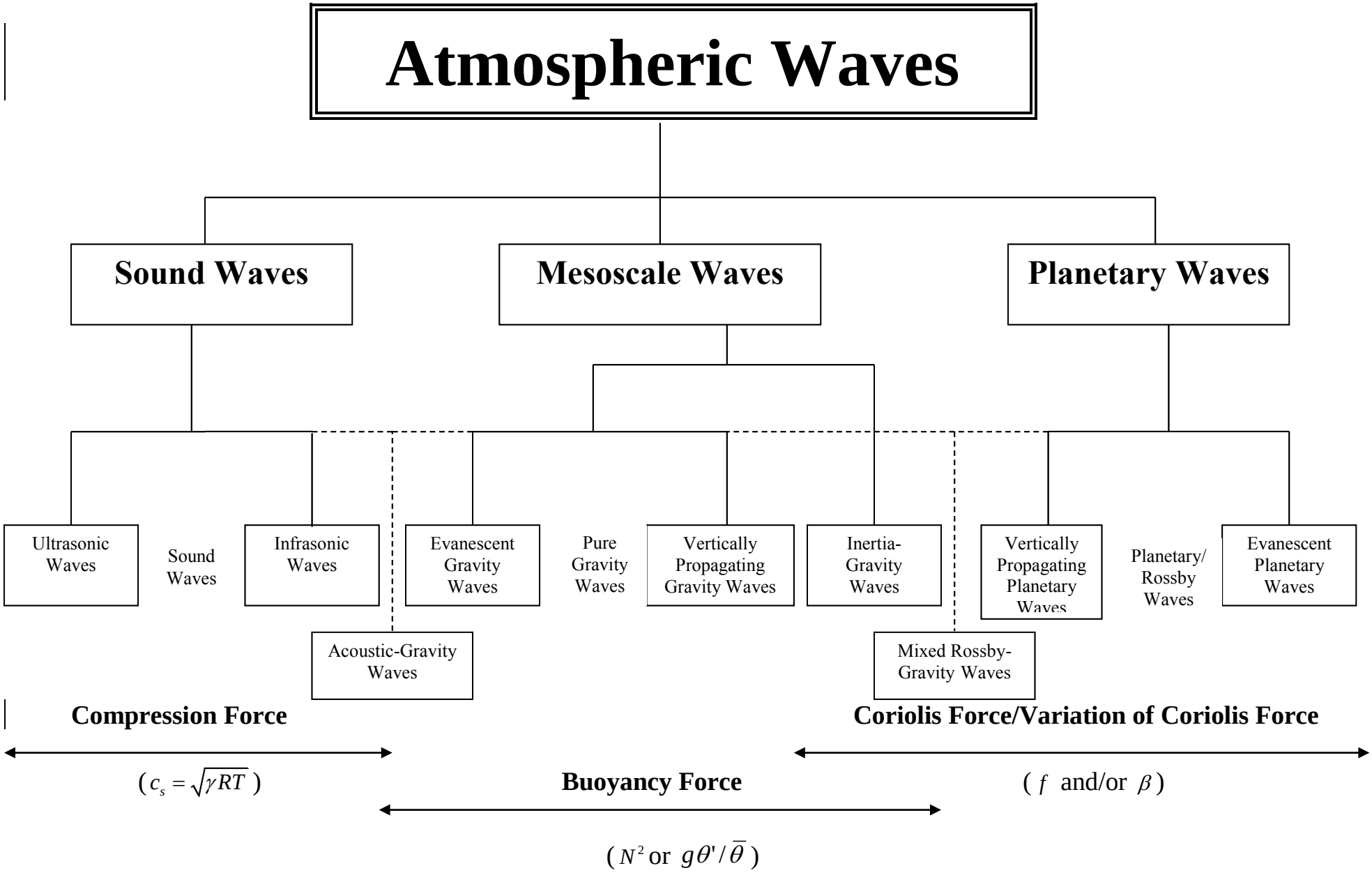
Atmospheric Waves
Sound Waves
Mesoscale Waves
Planetary Waves
Ultrasonic Waves
Sound Waves
Infrasonic Waves
Acoustic-Gravity Waves
Evanescent Gravity Waves
Pure Gravity Waves
Vertically Propagating Gravity Waves
Inertia-Gravity Waves
Mixed Rossby-Gravity Waves
Vertically Propagating Planetary Waves
Planetary/ Rossby Waves
Evanescent Planetary Waves
Compression Force
($c_s = \sqrt{\gamma RT}$)
Buoyancy Force
(N^2 or $g\theta'/\bar{\theta}$)
Coriolis Force/Variation of Coriolis Force
(f and/or β)

Table 3.1: A summary of atmospheric waves

Table 3.2: Dispersion relations and approximated equations of *w'* for mesoscale waves in different flow regimes

The governing equation for a linear, adiabatic, Boussinesq flow with a uniform basic state wind (U) and stratification (N) can be written:

$$\left(\frac{\partial}{\partial t}+U\frac{\partial}{\partial x}\right)^2\left(\frac{\partial^2 w'}{\partial x^2}+\frac{\partial^2 w'}{\partial y^2}+\frac{\partial^2 w'}{\partial z^2}\right)+f^2\frac{\partial^2 w'}{\partial z^2}+N^2\left(\frac{\partial^2 w'}{\partial x^2}+\frac{\partial^2 w'}{\partial y^2}\right)=0. \qquad (3.6.6)$$

The dispersion relation is

$$m^2=\frac{K^2(N^2-\Omega^2)}{\Omega^2-f^2};\ \Omega=\omega-kU, \qquad (3.6.10)$$

and three major flow regimes are

(I) High-frequency evanescent flow regime ($\Omega^2>N^2>f^2$; m imaginary)

(i) Potential (irrotational) flow ($\Omega^2>>N^2>f^2$)

$$m^2\approx -K^2;\qquad \left(\frac{\partial}{\partial t}+U\frac{\partial}{\partial x}\right)^2\left(\frac{\partial^2 w'}{\partial x^2}+\frac{\partial^2 w'}{\partial y^2}+\frac{\partial^2 w'}{\partial z^2}\right)=0, \qquad (3.6.12)$$

(i) Nonrotating evanescent flow ($\Omega^2>N^2>>f^2$ and O(Ω)=O(N))

$$m^2\approx -K^2\left(1-\frac{N^2}{\Omega^2}\right);\ \left(\frac{\partial}{\partial t}+U\frac{\partial}{\partial x}\right)^2\left(\frac{\partial^2 w'}{\partial x^2}+\frac{\partial^2 w'}{\partial y^2}+\frac{\partial^2 w'}{\partial z^2}\right)+N^2\left(\frac{\partial^2 w'}{\partial x^2}+\frac{\partial^2 w'}{\partial y^2}\right)=0$$

(II) Vertically propagating wave regime ($N^2>\Omega^2>f^2$; m real)

(i) Pure gravity waves ($N^2>\Omega^2>>f^2$ and O(N) =O(Ω))

$$m^2\approx K^2\left(\frac{N^2}{\Omega^2}-1\right);\quad \left(\frac{\partial}{\partial t}+U\frac{\partial}{\partial x}\right)^2\left(\frac{\partial^2 w'}{\partial x^2}+\frac{\partial^2 w'}{\partial y^2}+\frac{\partial^2 w'}{\partial z^2}\right)+N^2\left(\frac{\partial^2 w'}{\partial x^2}+\frac{\partial^2 w'}{\partial y^2}\right)=0 \qquad (3.6.14)$$

(ii) Hydrostatic gravity waves ($N^2>>\Omega^2>>f^2$)

$$m^2=\left(\frac{KN}{\Omega}\right)^2;\qquad \left(\frac{\partial}{\partial t}+U\frac{\partial}{\partial x}\right)^2\frac{\partial^2 w'}{\partial z^2}+N^2\left(\frac{\partial^2 w'}{\partial x^2}+\frac{\partial^2 w'}{\partial y^2}\right)=0, \qquad (3.6.16)$$

(iii) Hydrostatic inertia-gravity waves ($N^2>>\Omega^2>f^2$ and O(Ω) = O(f))

$$m^2 = \frac{K^2 N^2}{\Omega^2 - f^2}; \qquad \left[\left(\frac{\partial}{\partial t} + U\frac{\partial}{\partial x}\right)^2 + f^2\right]\frac{\partial^2 w'}{\partial z^2} + N^2\left(\frac{\partial^2 w'}{\partial x^2} + \frac{\partial^2 w'}{\partial y^2}\right) = 0, \quad (3.6.18)$$

(III) Low-frequency evanescent flow regime ($N^2 > f^2 > \Omega^2$; m□ imaginary)

(i) Quasi-geostrophic flow ($N^2 > f^2 >> \Omega^2$)

$$m^2 \approx \frac{-K^2 N^2}{f^2}; \qquad f^2\frac{\partial^2 w'}{\partial z^2} + N^2\left(\frac{\partial^2 w'}{\partial x^2} + \frac{\partial^2 w'}{\partial y^2}\right) = 0. \quad (3.6.20)$$

Figures

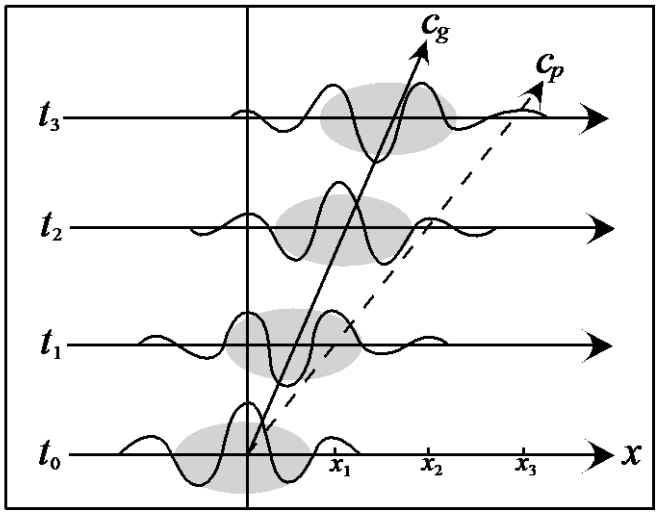

Fig. 3.1: Propagation of a wave group and an individual wave. The solid and dashed lines denote the group velocity (c_g) and phase velocity (c_p), respectively. Shaded oval denotes the concentration of wave energy which propagates with the group velocity. The phase speed c_p equals x_i / t_i, where i = 1, 2, or 3.

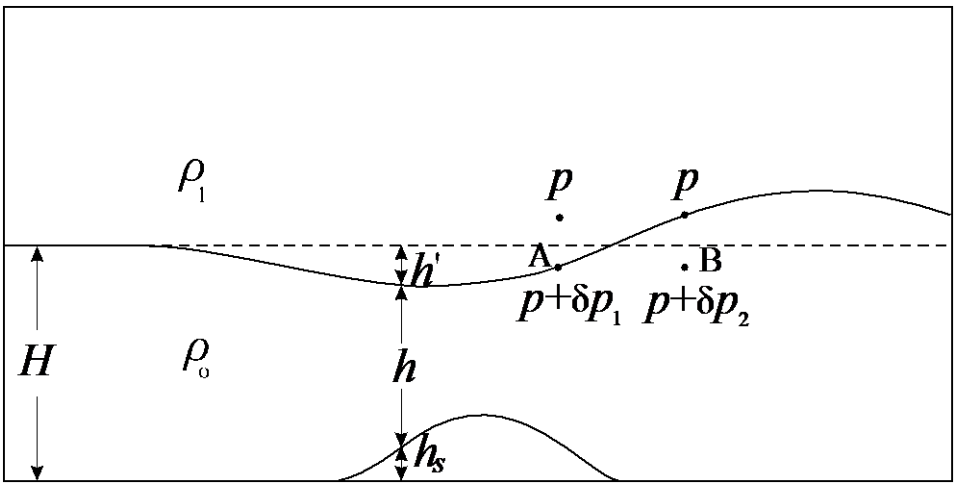

Fig. 3.2: A two-layer system of homogeneous fluids. Symbols H, h, h_s, and h' denote the undisturbed fluid depth, actual fluid depth, bottom topography, and perturbation (vertical displacement) from the undisturbed fluid depth, respectively. The densities of the upper and lower layers are ρ_1 and ρ_o, respectively. The pressure perturbations at A and B from p in the upper layer are denoted by $p + \delta p_1$ and $p + \delta p_2$, respectively.

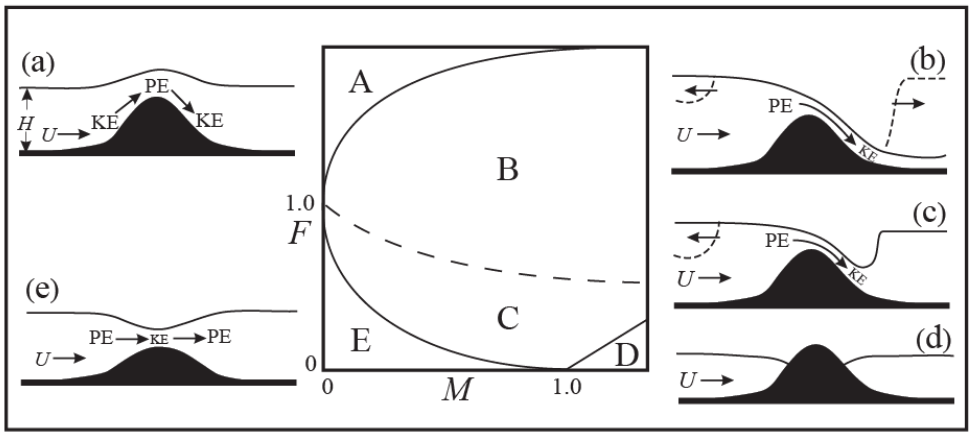

Fig. 3.3: Five flow regimes of the transient one-layer shallow water system, based on the two nondimensional control parameters ($F = U/\sqrt{gH}$, $M = h_m/H$). (a) Regime A: supercritical flow, (b) Regime B: flow with both upstream and downstream propagating hydraulic jump, (c) Regime C: flow with upstream propagating jump and downstream stationary jump, (d) Regime D: completely blocked flow, and (e) Regime E: subcritical flow. The dashed lines in (b) and (c) denote transient water surface. In regimes B and C, upstream flow is partially blocked. (Adapted after Baines 1995 and Durran 1990)

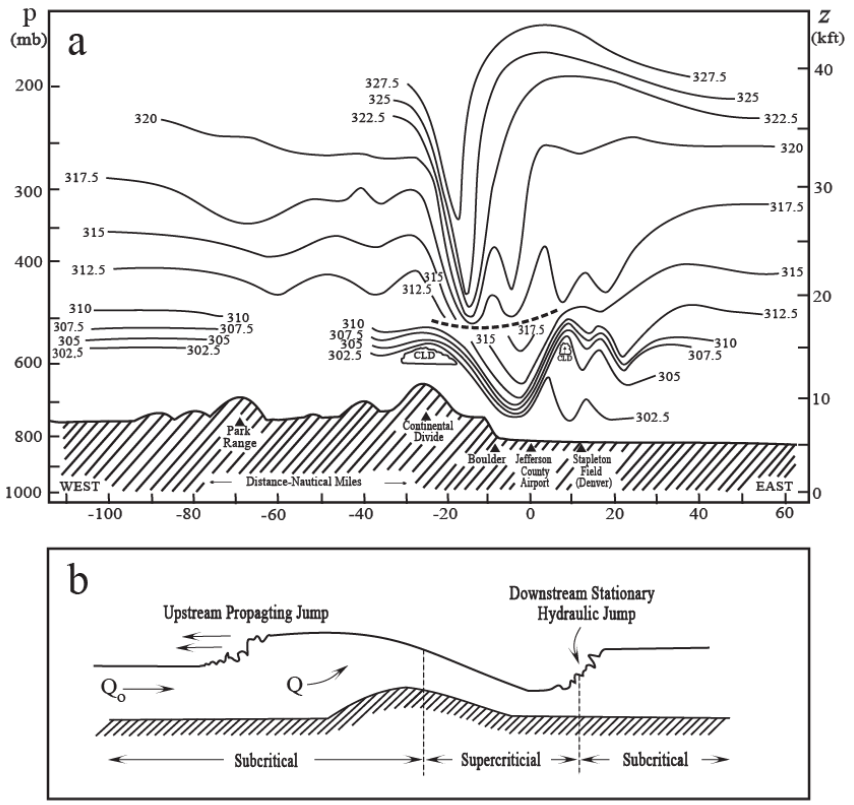

Fig. 3.4: (a) Analysis of potential temperature from aircraft flight data and rawinsondes for the 11 January 1972 Boulder windstorm. The bold dashed line separates data taken from the Queen Air aircraft (before 2200 UTC) and from the Saberliner aircraft (after 0000 UTC) (Adapted after Klemp and Lilly 1975). The severe downslope wind reached a speed greater than 60 ms^{-1}. (b) A sketch of flow Regime C of Fig. 3.3(c), which may be used to explain the phenomenon associated with (a). Q is the volume flux per unit width. (Adapted after Turner 1973)

Fig. 3.5: An internal hydraulic jump associated with a severe downslope windstorm formed along the eastern Sierra Nevada (to the right) and Owens Valley, California. The hydraulic jump was made visible by the formation of clouds and by dust raised from the ground in the turbulent flow behind the jump. (Photographed by Robert Symons)

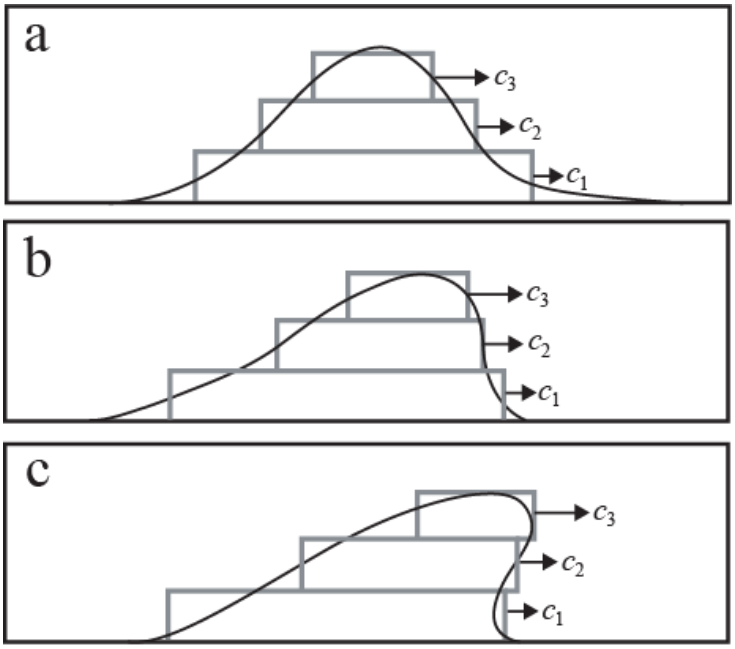

Fig. 3.6: The evolution of an initial symmetric wave, which is imagined to be composed of three rectangular blocks with shorter blocks on top of longer blocks. The wave speeds of these fluid blocks are approximately equal to $c_n = \sqrt{g(H+nh)}$, based on shallow-water theory, where n = 1, 2, and 3, H is the shallow-water layer depth, and h is the height of an individual fluid block. The wave steepening in (b) and wave overturning in (c) are interpreted by the different wave speeds of different fluid blocks because $c_3 > c_2 > c_1$.

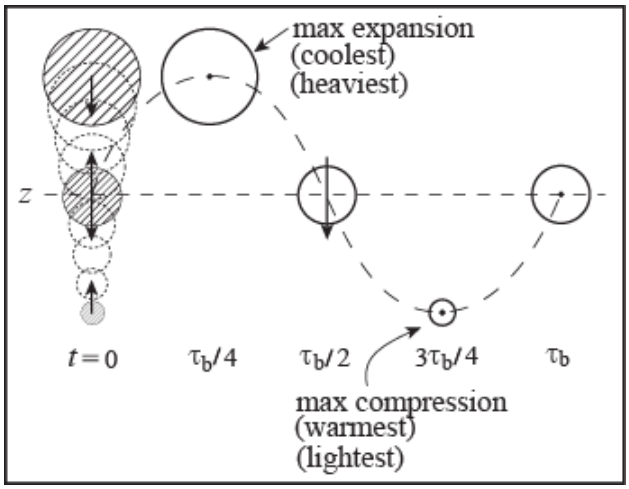

Fig. 3.7: Vertical oscillation of an air parcel in a stably stratified atmosphere when the Brunt-Vaisala frequency is *N*. The oscillation period of the air parcel is $\tau_b = 2\pi / N$ and the volume of the air parcel is proportional to the area of the circle. (Adapted after Hooke 1986)

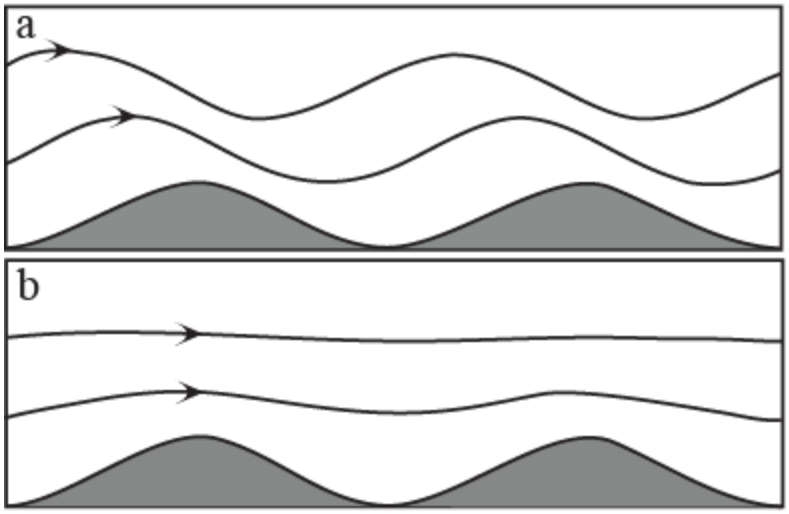

Fig. 3.8: (a) Vertically propagating waves and (b) evanescent waves for a linear, two-dimensional, inviscid flow over sinusoidal topography.

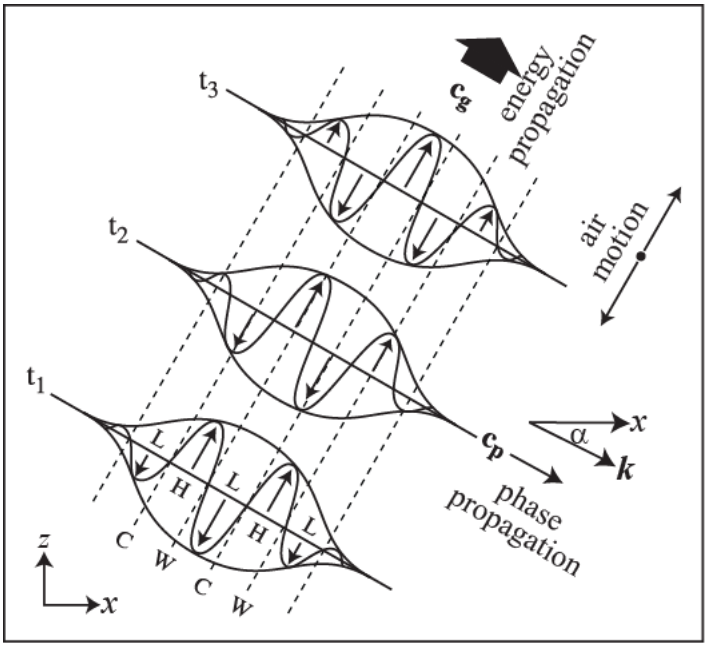

Fig. 3.9: Basic properties of a vertically propagating gravity wave with $k > 0, m < 0,$ and $\omega > 0$. The energy of the wave group propagates with the group velocity ($\boldsymbol{c_g}$, thick blunt arrow), while the phase of the wave propagates with the phase speed ($\boldsymbol{c_p}$). Relations between *w', u', p',* and θ' as expressed by (3.5.16) and (3.5.17) are also sketched. Symbols H and L denote the perturbation high and low pressures, respectively, while W and C denote the warmest and coldest regions, respectively, for the wave at t_1. Symbol α defined in (3.5.13) represents the angle of the wave number vector $\boldsymbol{k}$ from the horizontal axis or the wave front (line of constant phase) from the vertical axis. (Adapted after Hooke 1986)

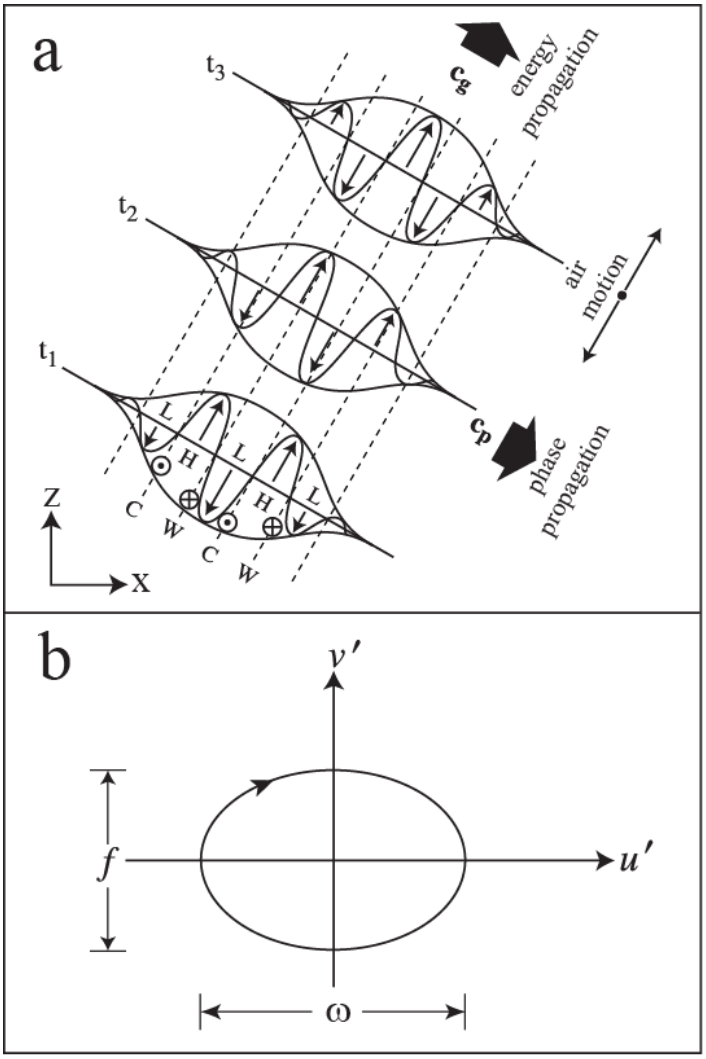

Fig. 3.10: (a) Similar to Fig. 3.9, except for a hydrostatic inertia-gravity wave with $m < 0$, $k > 0$, $l = 0$, $\omega > 0$, and $f > 0$. Meridional (i.e. north-south) perturbation wind velocities (v') are shown by arrows pointed into and out of the page. (b) The projection of fluid particle motion associated with a hydrostatic inertia-gravity wave onto the horizontal plane is an ellipse with ω/f as the ratio of major and minor axes. The velocity vector associated with a plane inertia-gravity wave rotates anticyclonically in the Northern Hemisphere with height for upward energy propagation. (Adapted after Hooke 1986)

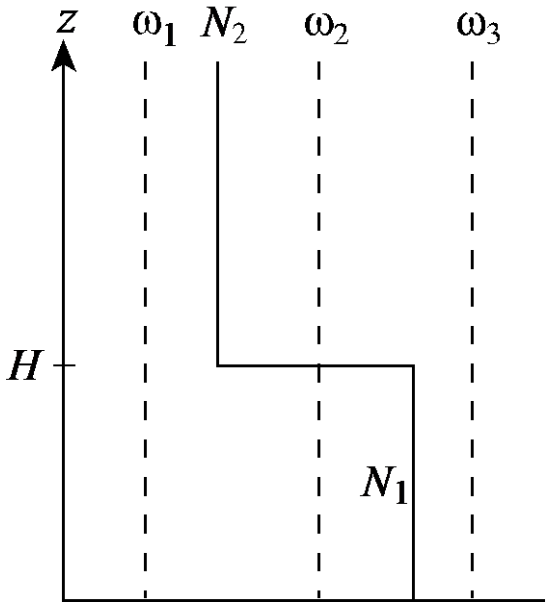

Fig. 3.11: Examples of wave reflection in a stratified flow with a piecewise constant profile in Brunt-Vaisala frequency (N). Case ω_1 has wave solutions in both layers; Case ω_2 has wave solutions in the lower layer, evanescent solutions in upper layer; and Case ω_3 has evanescent solutions in both layers. The forcing is assumed at $z = 0$.

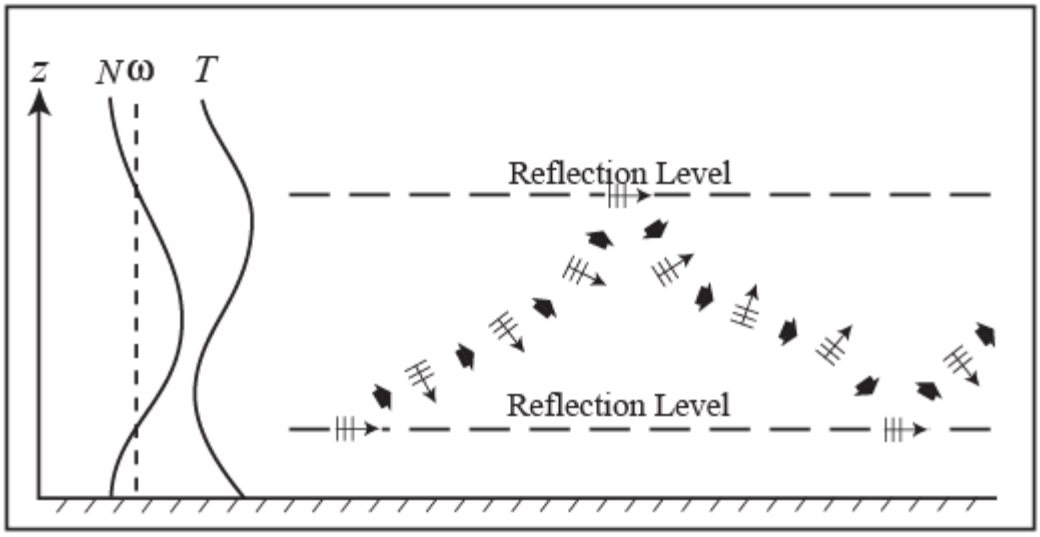

Fig. 3.12: Wave reflection in a continuously stratified fluid. *N* and *T* are the Brunt-Vaisala frequency and temperature of the sounding, respectively, and ω is the wave frequency. Ray paths are reflected at the reflection level at which $\omega = N$. A wave packet is also depicted in the figure. The short blunt arrows and long thin arrows denote the group and phase velocities, respectively, of the wave packet. Particle motions are parallel to the constant phase lines or wave fronts, which become vertically oriented at the reflection level since α, defined in (3.5.13) and also illustrated in Fig. 3.9, approaches 0. (Adapted after Hooke 1986)

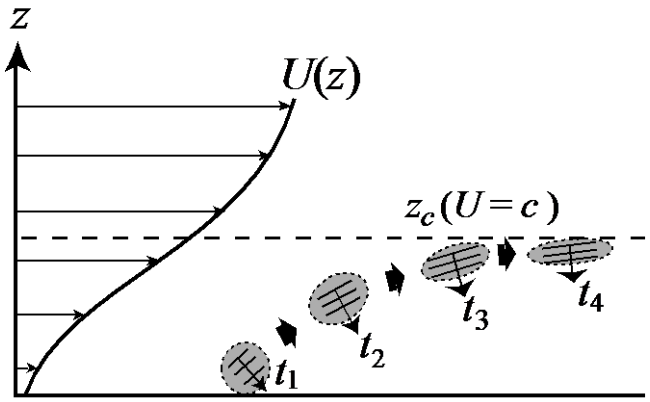

Fig. 3.13: The propagation of a wave packet upward toward a critical level located at $z = z_c$. The particle motions are parallel to the wave crests, which are denoted by straight lines. Note that the vertical wavelength decreases as the wave packet approaches the critical level. The phase lines are horizontally oriented at the critical level in this case. (Adapted after Bretherton 1966)

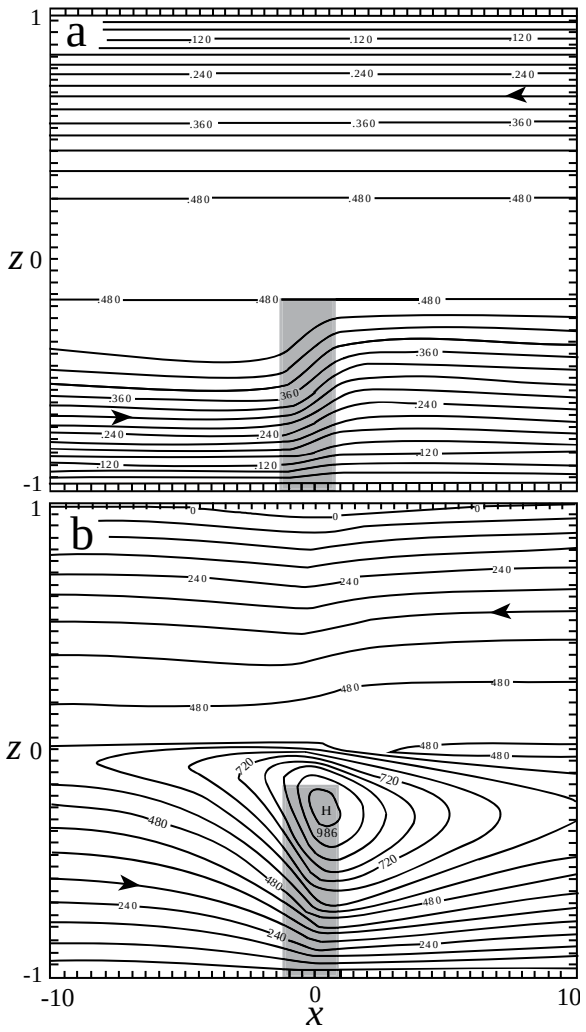

Fig. 3.14: (a) Streamlines for a linear, steady-state stratified airflow over an isolated heat source. The concentrated heating region is shaded. The basic flow has a linear shear (U_z = constant) and its Richardson number (Ri) is 10. (b) Same as (a) except for Ri = 1. All contour values are nondimensionalized. The streamfunction (ψ) used for constructing the streamlines is defined as $u = \partial\psi / \partial z$ and $w = -\partial\psi / \partial x$. (After Lin 1987)